Ship-borne aerosol profiling with lidar over the Atlantic Ocean: From pure marine conditions to complex dust-smoke mixtures.

Stephanie Bohlmann[1,2], Holger Baars[1], Martin Radenz[1], Ronny Engelmann[1], and Andreas Macke[1]

[1]Leibniz Institute for Tropospheric Research, Permoserstraße 15, 04318 Leipzig, Germany
[2]now at: Finnish Meteorological Institute, P.O. Box 1627, 70211, Kuopio, Finland
Correspondence to: Stephanie Bohlmann (stephanie.bohlmann@fmi.fi)

Abstract. The multiwavelength Raman lidar Polly[XT] have been regularly operated aboard the research vessel Polarstern on expeditions across the Atlantic Ocean from North to South and vice versa. The lidar measurements of the Polarstern cruises PS95 from Bremerhaven to Cape Town (November 2015) and PS98 from Punta Arenas to Bremerhaven (April/May 2016) are presented and analysed in detail. The latest setup of Polly[XT] allows improved coverage of the marine boundary layer (MBL) due to an additional near-range receiver.

Three case studies provide an overview of the detected aerosol over the Atlantic Ocean. In the first case, marine conditions were observed near South Africa on the autumn cruise PS95. Values of optical properties (depolarisation ratios close to zero, lidar ratios of 23 sr at 355 nm and 532 nm) within the MBL indicate pure marine aerosol. A layer of dried marine aerosol, indicated by an increase of the particle depolarisation ratio to about 10 % at both wavelengths and thus confirming the non-sphericity of these particles, could be detected on the top the MBL. On the same cruise, an almost pure Saharan dust plume was observed near the Canary Islands, presented in the second case. The third case deals with several layers of Saharan dust partly mixed with biomass-burning smoke measured on PS98 near the Cape Verde Islands. While the MBL was partly mixed with dust in the pure Saharan dust case, an almost marine MBL was observed in the third case.

A statistical analysis showed latitudinal differences in the optical properties within the MBL, caused by the down-mixing of dust in the tropics and anthropogenic influences in the northern latitudes whereas the optical properties of the MBL in the southern hemisphere correlate with typical marine values. The particle depolarisation ratio of dried marine layers ranged between 4–9 %.

Night measurements from PS95 and PS98 were used to illustrate the potential of aerosol classification using lidar ratio, particle depolarisation ratio and Ångström exponent. Lidar ratio and particle depolarisation ratio have been found to be the main indicator for the particle type, whereas the Ångström exponent is rather variable.

1 Introduction

Aerosols, solid or liquid particles dispersed in air, play an important role in the Earth's climate system. By scattering and absorbing solar and terrestrial radiation, aerosols highly affect the radiation fluxes and thus the radiative budget. Besides this direct aerosol radiative forcing, aerosols also modify the microphysical properties of clouds by acting as cloud condensation or

ice nuclei, and thereby influence the radiative budget indirectly (Twomey-effect (Twomey, 1977)). Furthermore, the presence of aerosol particles influence the lifetime of clouds (cloud lifetime effect (Albrecht, 1989)).

As the impact of aerosols on the climate system is various, it has to be considered in climate modelling to receive accurate results. Which is, however, challenging because not all aerosol types contribute to the aerosol radiative forcing in the same way
5 (Ocko et al., 2012; Myhre et al., 2013) and additionally, information about global aerosol distributions are rare due to their high spatial and temporal variability. Thus, uncertainties in aerosol forcing and the poor understanding of aerosol-cloud interactions represent a large uncertainty in current climate models despite the progress in observing and modelling climate-relevant aerosol properties and atmospheric distributions in the last years (IPCC, 2013). More information about the horizontal and vertical distribution of different aerosol types is needed to further improve climate modelling and prediction and to understand its
10 complex interaction with the atmosphere. Therefore, the observation of the spatio-temporal aerosol distribution is an objective in a wide range of research projects. But they mostly concentrate on observations over land. Since about 70 % of the Earth's surface is covered by water, aerosols and their distribution have to be investigated over the oceans as well even though the investigation is more challenging.

Light detection and ranging (LIDAR) represents a key method to investigate aerosols vertically resolved. Measurements with
15 high spatial and temporal resolution and under ambient conditions are possible up to an altitude of 100 km depending on the lidar setup (Wandinger, 2005). Many institutes all over the world are performing lidar measurements and create networks as shown in the 178th GAW report (Bösenberg et al., 2007). While the northern hemisphere is well covered with observation sites, there are only a few lidar stations on the southern hemisphere. Over the oceans aerosol measurements are rare and to our knowledge no regular vertically resolved measurements allowing aerosol typing are performed from ground. To close this gap,
20 the OCEANET project was initiated to investigate the transport of material and energy between ocean and atmosphere. The OCEANET project is a collective project of several German research institutes and combines oceanographic measurements with atmospheric observations on a ship-borne platform. It is regularly part of expeditions on research vessels (RV) like the RV Polarstern. One instrument within the OCEANET facility is the portable and automated Raman and polarisation lidar system Polly[XT] (Althausen et al., 2009; Engelmann et al., 2016). This lidar system allows aerosol typing and investigations of the
25 atmosphere up to about 20 km.

The first cruise with Polly[XT] on the RV Polarstern took place in 2009. Since then, eight cruises have been performed on the RV Polarstern between Bremerhaven and Punta Arenas and Bremerhaven and Cape Town until summer 2016, covering almost the whole north-south extension of the Atlantic Ocean. These measurements therefore represent a valuable contribution to the comprehension of the aerosol distribution over the Atlantic. These Polly[XT] Polarstern cruises are listed in Table 1, which also
30 gives information on the used lidar system. The cruise tracks are presented in Fig. 1. The first three cruises ANT-XXVI/1, ANT-XXVI/4 and ANT-XXVII/1 have already been analysed by Kanitz (2012). Saharan dust and mixtures of biomass-burning smoke and dust were observed at the west coast of North Africa as well as Patagonian dust over the South Atlantic. The used lidar system did not cover the lower most 500–800 m of the troposphere, therefore the marine boundary layer (MBL) could not be investigated. However, the investigation of optical and microphysical properties of pure marine aerosol is essential, as this
35 knowledge is used in retrievals for space-borne instruments like CALIPSO (Omar et al., 2009) which are able to investigate

aerosols globally and thus also over the ocean but with limited capabilities. As land-based observations of aerosols mostly do not allow to observe pure marine conditions only shipborne observations are suited to make detailed studies of the marine environment found over the oceans which are needed to support the global observations of the space-borne lidars (Omar et al., 2009). Polly^{XT} has been further developed since these first cruises to meet these requirements. The latest setup (Engelmann

5   et al., 2016) possesses now, additionally to the original capabilities, four near-range channels and depolarisation measurements at two wavelengths. Due to a new near-range detection unit, the height of complete overlap between receiver field-of-view and laser beam was reduced from about 1500 m to 120 m and now enables measurements close to the lidar. Observations with this advanced lidar setup over the ocean offer the unique opportunity to investigate the MBL in addition to the aerosol conditions in the free troposphere, which was not possible until now. Three typical case studies will be discussed and a statistical analysis of

10   the two cruises is presented contrasting the zonal dependence of the aerosol conditions over the Atlantic. This paper therefore focusses on the analysis of the two recent cruises, namely PS95 and PS98, to investigate the whole atmospheric column above the ship.

The paper is structured as follows, in Sec. 2 the Raman-lidar Polly^{XT} and the aerosol characterisation by optical properties is briefly introduced and an overview of the lidar measurements during PS95 and PS98 is given. In Section 3 three case studies

15   are discussed. A statistical analysis of both cruises are given in Sec.4. In Section 5 the results are summarised.

2 Experiment

2.1 Lidar measurements

The lidar measurements during the Atlantic cruises were performed with the portable Raman and polarisation lidar system Polly^{XT}-OCEANET. A detailed description of the optical setup can be found in Althausen et al. (2009) and Engelmann et al.

20   (2016).

The latest setup of Polly^{XT}-OCEANET enables the measurement of backscatter coefficient profiles at 355, 532 and 1064 nm and extinction coefficient profiles at 355 nm and 532 nm. Furthermore, depolarisation measurements at 355 nm and 532 nm are possible. A second detection unit enables measurements near the lidar at 355 nm and 532 nm and the corresponding Raman wavelengths 387 nm and 607 nm down to about 120 m above the lidar (Engelmann et al., 2016).

25   The backscatter coefficient β describes the amount of the light backscattered to the lidar at an angle of 180°. The attenuation of the emitted light due to absorption and scattering on the way through the atmosphere is described by the extinction coefficient α. The ratio of extinction to backscatter coefficient is called lidar ratio S. As the extinction is the attenuation of light due to scattering and absorption, the lidar ratio can be used to determine the absorbing capacity of the backscattering particles. Absorbing aerosols like soot have a much higher lidar ratio than non-absorbing particles like sea salt (Müller et al., 2007; Groß

30   et al., 2011). The relationship of the backscatter or extinction coefficient at two wavelengths λ_1, λ_2 as a function of the ratio of these wavelengths is given by the backscatter or extinction-related Ångström exponent $\mathring{A}$ (Ångström, 1929). It indicates the particle size. Small particles show a strong wavelength dependence, thus $\mathring{A}$ is greater than 1. In contrast, the scattering on large particles is almost wavelength independent and $\mathring{A}$ is approximately zero (Eck et al., 1999; Müller et al., 2007; Baars et al.,

2016).

The emitted laser light of the Polly^{XT} lidar is linear polarised. In the atmosphere, the light is depolarised while scattered at non-spherical particles like dust or ice crystals. The detected light therefore contains a cross-polarised component in addition to the parallel polarised light and can be detected separately. The ratio of cross-polarised to parallel-polarised light backscattered

5 by particles is called particle depolarisation ratio. If the particles are mainly spherical, the particle depolarisation ratio is about zero because the linear polarised light has been reflected to the lidar without changing the polarisation shape within the particle or its edges. The particle depolarisation ratio increases with non-spherical shape and therefore enable the determination of the particle sphericity.

Ångström exponent, lidar ratio and depolarisation ratio are indicators of the aerosol type. By knowing typical values of the
10 lidar ratio, Ångström exponent and particle depolarisation ratio, the optical dominant particle type can be specified.

2.2 Lidar observations during Polarstern cruises across the Atlantic

The temporal development of the range-corrected signal (i.e. the uncalibrated attenuated backscatter signal) of the autumn transit cruise PS95 is shown in Fig. 2 (middle panel). Polarstern departed on 29 October 2015 from Bremerhaven and arrived
15 on 1 December 2015 at Cape Town. The first days of this cruise were characterised by low-level clouds and rain indicated by white colours. On 9 November (33° N), the lidar could detect a lofted plume of Saharan dust above the MBL between 600 m and 3 km height. From 12 November (24° N), increasing depolarisation in the MBL could be observed ((lower panel Fig. 2) resulting from deposition and downmixing of dust from higher altitudes. The dust top height decreased from 2.8 km on 11 November down to 1.5 km on 13 November. About noon on 14 November 2015, a new dust plume with a lower volume de-
20 polarisation ratio and a dust top height of 3.5 km was observed. Polarstern steadily moved towards the equator so that the dust region was left behind in the night to 18 November (3° N). After entering the southern hemisphere on 19 November, marine stratocumulus clouds occurred frequently. Around noon on 23 November (10° S), minor traces of dust between 1 km and 4 km could be observed again. Considering HYSPLIT trajectories (not shown), these depolarising layers could consist of dust from the Kalahari Desert. From 24 November (12° S) onwards, the sky was mostly overcast. At the end of the cruise, on 29 and 30
25 November, almost pure marine conditions could be observed. The 500 nm AOT, measured with a Microtops sunphotometer, ranged around 0.1 on the northern hemisphere, increased in the dust influenced northern tropics to around 0.5 and decreased below 0.1 in the southern hemisphere.

The spring transit cruise PS98 started on 11 April 2016 in Punta Arenas (Chile) and ended on 11 May 2016 in Bremerhaven. The time series of the range corrected signal and volume depolarisation ratio at 532 nm are shown in Fig. 3. Because of a
30 failure of the 1064 nm photomultiplier tube (PMT) no measurements at this wavelength were available. After starting regular measurements in the night to 13 April, the weather was dominated by clouds. In the night from 14 to 15 April (40° S), thin depolarising layers at around 2.5 km could be observed. According to HYSPLIT backward trajectories (not shown), the air-mass originated from the Patagonian region, thus the layers could contain traces of Patagonian dust. Observations on 16 and 17 April were dominated by low clouds and rain. From 22 April (12° S) to 25 April (4° S), a lofted dust plume between 1.5 km

and 3.5 km height could be detected. Crossing the Intertropical Convergence Zone (at around 5° N) on the 27 and 28 April, thunderstorms, rain showers and clouds with low base heights were predominant. After leaving this region, the lidar observed Saharan dust above the marine boundary layer again. The bottom height of the dust layer decreased from 1.5 km on 22 April down to around 600 m on 30 April. In the afternoon of 1 May (23° N), Polarstern left the dust region. After a short stop at the port of Las Palmas (Gran Canaria, Spain) on 3 May, the cruise was continued towards the European continent and the aerosol conditions were more and more influenced by anthropogenic sources. From 6 May onwards, mostly overcast sky with small cloud gaps was predominant. The AOT at 500 nm showed a similar zonal behaviour as on the PS95 cruise. The AOT at 500 nm was below 0.1 in the southern hemisphere, except for the 17 April, and steadily increased to the maximum of 0.37 on 30 April. After leaving the dust influenced region, the AOT ranged between 0.1–0.2 on the northern hemisphere.

Regular cruises across the Atlantic Ocean from North to South in the northern hemispheric autumn and from South to North in the northern hemispheric spring provided a large amount of lidar data over the Atlantic. Dust is regularly observed in the northern tropics and subtropics west of the Saharan desert. The AOT at 500 nm, measured with a Microtops sun photometer, is slightly higher on the northern than on the southern hemisphere which indicates a higher aerosol load on the northern hemisphere.

3 Results

3.1 Case studies

Three night measurements from PS95 and PS98 were selected to present typical atmospheric conditions by means of a detailed discussion of the optical properties in the MBL and in lofted layers. First, almost pure marine conditions with an overlying dried marine aerosol layer during the autumn cruise PS95 are discussed. Second, a case study on the same cruise but with Saharan dust near the Canary Islands is presented. Third, a case during the spring cruise 2016 (PS98) with a mixture of Saharan dust and biomass-burning aerosol mixtures near the Cape Verde Islands is shown. These three case studies are marked white in the cruise overviews (Fig. 2 and Fig. 3).

3.1.1 PS95 - Marine aerosol conditions

At the end of the cruise PS95 on 29 and 30 November 2015 near Cape Town, marine conditions could be observed. In Figure 4, the time series of the range-corrected signal at 1064 nm and the volume depolarisation ratio at 532 nm from 29 and 30 November 2015 are shown. Additionally, the AOT at 500 nm and the Ångström exponent at 440/870 nm retrieved by sun photometer measurements are shown in the upper panel. Mean AOT at 500 nm of 0.09±0.01 on 29 November (0.09±0.02 on 30 November) and an Ångström exponent of 0.08±0.02 (0.23±0.08) clearly indicate marine conditions for remote oceanic areas, not influenced by continental aerosol sources. In these regions, the AOT at 500 nm is typically below 0.1 and $Å≈0.6$

(MAN, Smirnov et al., 2009).

The time series of the volume depolarisation ratio shows a thin layer of enhanced depolarisation at the top of the MBL at 300–400 m. This layer consists of dried marine particles and will be discussed later in this Section.

Mean profiles of the measured optical properties are shown in Fig. 5 for 30 November 01:15–02:30 UTC with a vertical smooth-ing length of 127.5 m. For extinction coefficient, lidar ratio and Ångström exponent profiles, a smoothing length of 127.5 m in the boundary layer and 457.5 m above 340 m height was used to reduce signal noise. Nevertheless, high signal noise does occur in the extinction coefficient profile above 500 m due to the very low aerosol concentrations. Such noisy profiles will be cut off in the following examples as the lidar is not sensitive enough and correspondingly the signal-to-noise ratio is too low in regions of such low (almost zero) extinction coefficients. In the right panel, GDAS1 and radio sounding profiles are shown. GDAS1 data represent temperature and relative humidity profiles at 0 UTC, whereas the radio sounding profile represents atmospheric conditions at 12 UTC.

According to the backscatter coefficient and the GDAS1 and sounding profile in Fig. 5, the MBL top height was only about 300 m. Within the MBL, the lidar ratio was 23±2 sr at 355 nm and 23±1 sr at 532 nm, which agrees with results during the second Aerosol Characterization Experiment ACE-2 (S_{532} 23±3 sr (Müller et al., 2007)) and are slightly higher than results of the Saharan Mineral Dust Experiment SAMUM-2a (S_{532} 18±4 sr and S_{355} 18±2 sr (Groß et al., 2011)).

The special highlight in this case study is the increase of the depolarisation ratio at the top of the MBL. The particle depolar-isation ratio at 355 nm and 532 nm are around zero in the MBL (large, non-depolarising particles) and increase from 300 m to about 450 m, shortly above the MBL top. After this peak, the depolarisation decreases to about zero again. Considering the profiles of relative humidity and temperature, a correlation with the relative humidity is obvious. The relative humidity (RH) decreases from about 90 % near the ground to under 20 % above 600 m. In the layer the RH is about 50 % according sounding data and about 40 % according to GDAS1. Simultaneously the temperature increases. HYSPLIT backward trajectories (Fig. 6) indicate that the air parcels arriving at 300, 600 and 1000 m had only been carried over the South Atlantic Ocean the last 7 days, thus it can be assumed that the airmass contains mostly marine aerosol originated from the ocean, e.g. sea salt. Sea salt aerosol exists as dry particles at low relative humidity. Since sea salt is hygroscopic, the salt particles absorb water to form droplets when the RH exceeds the deliquescence relative humidity (DRH). If the RH decreases to the crystallisation relative humidity (CRH), the particle crystallise from the droplet. At a RH above the CRH, the sea salt particles are in solution with water and show low values of $\delta \approx 3\,\%$ (Tesche et al., 2011a). When the RH is below the CRH, the sea salt particles crystallise and exist as non-spherical particles due to the cubic shape of NaCl, the main constitute of sea salt aerosol (Kokhanovsky, 2008). As non-spherical particles they cause higher depolarisation ratios. In this case, dried sea-salt particles caused depolarisation ratios up to 9 % at 532 nm and 10 % at 355 nm. Previous studies showed similar results. Murayama et al. (1999) measured high depo-larisation ratios ($\approx 10\,\%$) at 532 nm in the lower atmosphere associated with sea breeze events in the coastal area of Tokyo Bay. During the Saharan Aerosol Long-range Transport and Aerosol-Cloud-interaction Experiment (SALTRACE) winter campaign 2014 at Barbados, Haarig et al. (2017) detected an increase of the particle depolarisation ratio up to 12 % at 355 nm, 15 % at 532 nm and 10 % at 1064 nm when the RH drops below 50 %. Sakai et al. (2000) observed low depolarisation ratios (<5 %) at 532 nm over a wide range of relative humidities, whereas $\delta^{par} > 10\,\%$ was measured at low RH (<50 %) in air masses which

had passed over the Pacific Ocean. In a laboratory chamber experiment, Sakai et al. (2010) found linear depolarisation ratios at 532 nm of $1\pm \leq 0.1\,\%$ for droplets, $8\pm1\,\%$ for sea salt crystals and $21\pm2\,\%$ for NaCl crystals.

Thus, we can conclude that marine particles were transported above the MBL top, dried and crystallised and therefore cause a high particle depolarisation ratio even though the backscattering is low compared to the MBL.

5 The extinction and backscatter-related Ångström exponents are low in the MBL and increase above the layer with enhanced depolarisation ratio. Since low $Å$ is an indicator for large particles and higher $Å$ indicates small particles, the particles above the mentioned layer are smaller than the particles below, which is in good agreement with the hypothesis of the dried marine aerosol layer above the MBL.

This case confirms that marine aerosol can cause depolarisation in the lidar signal when RH is low. Without considering this
10 property of marine aerosol, aerosol layers above the MBL causing depolarisation may be falsely classified. Thus, automatic classification algorithms like the ones for CALIPSO, EarthCARE and other lidars should take these feature into account to not mis-classify these aerosols as, e.g., mixed dust.

3.1.2 PS95 - Saharan dust

When Polarstern approached the Canary Islands during the autumn cruise 2015, the first dust plume was observed in the
15 evening of 10 November at around 28° N. The dust could be measured until 14 November.

Figure 7 presents the column integrated concentration on 11 November 2015 12:00 UTC from the BSC-DREAM8b model (Dust REgional Atmospheric Model), operated by the Barcelona Supercomputing Center (http://www.bsc.es/ess/bsc-dust-daily-forecast, accessed: 14/11/1016). The increased column dust load above the Atlantic at the position of Polarstern is illustrated by the dark green colour. According to HYSPLIT backward trajectories (Fig. 8), the air mass measured on 11 November 20 UTC originated
20 from the Saharan desert. Only air masses that arrived at 3 km had been carried also over European areas in the last 7 days.

The range-corrected signal at 1064 nm and the 532 nm volume depolarisation ratio of the first dust plume are shown in Fig. 9. Additionally, sun photometer measurements from 11 and 12 November are given. The sun photometer retrieved Ångström exponent at 440/870 nm is 0.13 on 11 November and 0.08 for the day after. The daily averaged AOT at 500 nm for these days is 0.38 (11 November) and 0.58 (12 November). The dust layer reached heights about 3 to 3.5 km on 11 November and slightly
25 descended towards the 14 November. From 13 November lofted layers between 2–3.5 km with a lower depolarisation ratio than the first dust plume could be observed at around 3 km.

Averaged profiles of the measured optical properties and radio sounding and GDAS1 profiles of temperature and relative humidity are shown in Fig. 10 for 11 November 19:30–21:00 UTC (white frame Fig. 9). The backscatter coefficient profiles show an increased backscatter coefficient at all wavelengths up to 2.8 km above the MBL (top height 400 m). The 532 nm backscatter
30 coefficient is significantly larger than the 355 nm signal, whereas the extinction coefficient is wavelength independent. Even though, this is an untypical spectral behaviour, comparable observations of higher 532 nm than 355 nm backscatter coefficient were already observed in dust layers near the Cape Verde Islands (Rittmeister et al., 2017), in the eastern Mediterranean at Crete (Tsekeri et al., 2017) and during the SHADOW (Study of SaHAran Dust Over West Africa) campaign in Senegal (Veselovskii et al., 2016). According to Veselovskii et al. (2016), this spectral behaviour may be caused by specific refractive

index characteristics induced by the chemical composition of the particles. The mean lidar ratio at 532 nm (355 nm) in the height of the lofted aerosol layer is 53±2 sr (61±4 sr). The lidar ratio at 355 nm is higher than at 532 nm, which results from the higher backscatter coefficient at 532 nm and agrees with values found for dust during the SHADOW campaign (Veselovskii et al., 2016). Consequently, the mean backscatter-related 355/532 nm Ångström exponent is negative (-0.4±0.1). Negative

5 backscatter-related Ångström exponents are generally found when scattering properties of dust are modelled by assuming a spheroidal shape distribution. The values then typically vary between -0.5 and -2 depending on the assumptions of the spectral refractive index and the size and shape distributions. The extinction-related $\mathring{A}$ at 355/532 nm of 0.1±0.5 and the backscatter-related $\mathring{A}$ at 532/1064 nm of 0.4±0.1 are in good agreement with values for dust measured during SAMUM-2b ($\mathring{A}_{ext}^{355/532} \approx$ 0.22±0.27, $\mathring{A}_{bsc}^{532/1064} \approx$ 0.45±0.16 (Tesche et al., 2011a)). Furthermore, the aerosol layer between 600 m and 2.8 km is char-

10 acterised by a nearly height constant particle depolarisation ratio of 29±1 % at 532 nm and 25±1 % at 355 nm. The increased particle depolarisation ratios indicate a non-spherical particle shape and are in good agreement with values found for pure dust during SAMUM-2a ($\delta_{532}^{par} \approx 30\%$ and $\delta_{355}^{par} \approx 25\%$ (Groß et al., 2011; Tesche et al., 2011a)). The fraction of dust and smoke can be estimated using a method described by Tesche et al. (2009). Assuming a δ_{532}^{par} of 31 % for pure dust and 5 % for smoke, the fraction of dust in this layer amounts over 90 % (panel 6, Fig. 10) and can therefore be considered as pure dust.

15 The MBL reached a height of about 400 m according to the backscatter profile. Lidar ratios at 532 nm and 355 nm are 30±3 sr and 30±2 sr in the MBL, which are higher than the characteristic values for marine aerosol (see marine case study Sec. 3.1.1) and suggest a mixture of marine aerosol with other particles. The particle depolarisation ratios are also slightly higher, 9 % at 532 nm and 6 % at 355 nm, and indicate the mixing of dust into the MBL. Therefore also the MBL is influenced by the frequent dust emission in the Saharan desert.

20 ### 3.1.3 PS98 - Mixed aerosol layers

During the spring cruise PS98, extended aerosol layers with enhanced depolarisation were observed near the Cape Verde Islands. The range-corrected signal and volume depolarisation ratio at 532 nm as well as Microtops sun photometer measurements on 29 April 2016 are shown in Fig. 11.

An increased backscatter coefficient at both wavelengths indicates aerosol layers between 0.9–3 km. These layers are separated
25 from the MBL, which reached a height of about 500 m according to the increased backscatter signal and GDAS1/radio sounding data. The mean lidar ratio at 355 nm is 22±1 sr, the mean backscatter-related 355/532 Ångström exponent amount 0.9±0.0 and the mean particle depolarisation ratios are around zero at both wavelengths in the MBL. These values are indicators of a pure marine boundary layer without dust (see marine case, Sec. 3.1.1).

Regarding the backscatter profile, the aerosol-laden region above the MBL can be divided into four layers. The first layer
30 extends from 0.9–1.2 km, the second layer from 1.3–1.6 km, the third from 1.7–2.5 km and the fourth layer extends from 2.6–3.0 km.

Sun photometer measurements determined an average AOT at 500 nm of 0.23 and an Ångström-Exponent of 0.9 for 440/870 nm. Mean profiles of the optical properties averaged from 29 April 2016 between 20:15–21:00 UTC are shown in Fig. 12. The 532 nm near-range extinction coefficient and lidar ratio was not reliable because of a misalignment of the 532 nm near-range

channel which do not affect the Raman backscatter retrievals. The mean lidar ratio in the first layer is 48±4 sr and 46±9 sr at 532 nm and 355 nm, respectively. The mean backscatter-related 355/532 Ångström exponent is 0.4±0.1 and range between the typical values of dust (0.16±0.45, SAMUM-2b) and smoke (0.90±0.26, SAMUM-2a (Tesche et al., 2011b)). Same applies for the mean particle depolarisation ratio, which is 20±2 % at 532 nm and 15±2 % at 355 nm. These values are in good agreement

5 with values for dust and smoke mixtures measured during SAMUM-2a ($\delta^{par}_{355,532} \approx 16$ % (Tesche et al., 2011a)).

The second layer extends from 1.3–1.6 km. The mean lidar ratio is 57±7 sr and 63±8 sr at 532 nm and 355 nm, respectively. Mean backscatter and extinction-related $\mathring{A}$ at 355/532 nm amount 0.1±0.1 and 0.4±0.2, respectively. The mean particle depolarisation ratio of 24±2 % at 532 nm and 19±2 % at 355 nm suggest a mixture of depolarising dust ($\delta^{par}_{532} \approx 31$ % (Tesche et al., 2011)) and non-depolarising smoke ($\delta^{par}_{532} \approx 5$ % (Tesche et al., 2011a)). Applying the method described by Tesche et al.

10 (2009), the fraction of dust in this layer amounts up to 85 % (panel 6, Fig. 12).

In the third and fourth layer the extinction coefficient and therefore the lidar ratio show a significant wavelength dependence. The extinction at 355 nm is higher than at 532 nm. Lidar ratio and backscatter-related Ångström exponent in the third layer are comparable with values in the first layer. The mean lidar ratio at 532 nm amount 40±4 sr and 47±9 sr at 355 nm. The mean backscatter and extinction-related $\mathring{A}$ at 355/532 nm is 0.4±0.1 and 0.7±0.7, respectively. Whereas lidar ratio and Ångström

15 exponents remain nearly constant in this layer, the particle depolarisation ratio ($\delta^{par}_{532} \approx 19$ %) is significant higher at the top than at the base ($\delta^{par}_{532} \approx 11$ %). This may result from different aerosol sources, alterations during transport or mixing processes. The fourth layer is characterised by a high lidar ratio of 88±8 sr at 532 nm and 60±6 sr at 355 nm and high backscatter and extinction-related Ångström exponents of 0.6±0.1 and 1.6±0.3, respectively, which indicate the presence of large, absorbing particles. Mean particle depolarisation ratios of 13±3 % and 9±3 % at 532 nm and 355 nm also indicate an amount of depolar-

20 ising particles. Using the dust-smoke separation method described by Tesche et al. (2009), the fraction of dust amount around 36 %. The fraction of smoke is therefore significantly higher than in the other layers.

Figure 13 presents the HYSPLIT backward trajectories for the last 10 days arriving at the position of Polarstern at different altitudes. Air masses arriving in the MBL (500 m) had been carried only over the Atlantic Ocean the last 10 days and therefore contained mostly marine aerosol. Air masses arriving between 1–3 km were advected from the African continent. The air

25 masses arriving at 1 km height originated from the Saharan desert and passed over active fire areas south west of the Saharan desert 6 days before arriving at the position of Polarstern. Trajectories arriving at 1.5 km and 2 km also passed over the Saharan desert and active biomass-burning regions, but have never been close to the ground. As investigated by Nisantzi et al. (2014), fires can support the upward transport of dust into the free troposphere. A high amount of dust besides biomass-burning aerosol could therefore also be detected in these altitudes. In contrast, air masses arriving at 2.5 km and 3 km were on ground level over

30 active fire regions for several days and could take up a high amount of biomass-burning aerosol.

Summing up, one can state that during this night measurement, four layers with different fractions of dust and smoke could be detected. At the same time, the MBL was almost pure marine without mixed-in dust or smoke particles. This case study shows, the MBL is not always influenced by dust and smoke transport and that different aerosol types can occur at the same time above the Atlantic.

4 Statistical analysis

A statistical analysis of all analysed measurements was performed to provide an overview of latitudinal trends and characteristics of the different aerosol types observed over the Atlantic.

4.1 Time series

A total of 45 night measurements from PS95 and PS98 were selected for analysis with respect to optical aerosol properties using the Raman method. Each measurement was screened for separated aerosol layers. The MBL and, when present, elevated aerosol layers and layers of dried marine aerosol, as presented in the first case study, have been separately analysed. These layers with enhanced depolarisation ratio directly above the MBL are named dried marine layers from now on. The MBL top height and the extent of the analysed elevated aerosol layers and dried marine layers are shown in the first row of Fig. 14 for PS95 (left) and for the PS98 cruise (right), illustrated with blue dots and black and red bars, respectively. The MBL top height ranges between 300 m and 900 m and shows no significant latitudinal trend. Mean values of backscatter and extinction coefficient, lidar ratio and particle depolarisation ratio at 532 nm and the backscatter and extinction-related Ångström exponents are shown in the panels below. Measurements at 355 nm are not shown for the sake of clarity but show similar results. Blue dots illustrate the MBL mean values derived from near-range measurements. Mean values of the elevated aerosol layers are derived from far-range signals and are illustrated with black dots, whereas mean values of the dried marine layers are illustrated red. These mean values are derived from near range signals. An exception is the measurement at 22° S where the far-range signal is used because of the height of the dried marine layer. Error bars represent the standard deviation. For 27 measurements from 48° N to 31° S, the weather conditions and the instrument status allowed the analysis of the aerosol conditions over the Atlantic Ocean during PS95. The mean MBL backscatter coefficients range from 1.9–10 Mm^{-1}sr^{-1}, whereas the backscatter coefficient in the elevated layers is lower and ranges between 0.6–5 Mm^{-1}sr^{-1}. Mean extinction coefficients range between 38–323 Mm^{-1} at 532 nm in the elevated layers and 46–310 Mm^{-1} at 532 nm in the MBL. Mean backscatter and extinction coefficients of dried marine layers are only shown for the measurements at 31° S on 30 November 01:15–02:30 UTC, because of a low signal-to-noise ratio in the height of these layers in the other observed cases. The particle depolarisation ratio is given for all observed dried marine layers. Mean MBL lidar ratios at 532 nm are around 25±3 sr in the northern latitudes and 20±3 sr in the southern hemisphere. In the region of dust, between 35° N and the equator, the mean lidar ratio in the MBL is around 30±6 sr at 532 nm. The increased lidar ratio is caused by downmixing of dust from higher altitudes, whereas the lidar ratio in the southern latitudes correlates with pure marine values. Anthropogenic aerosol from the European continent influences the MBL in northern latitudes, the lidar ratio is therefore slightly higher than for a pure marine environment. The lidar ratio in the dried marine layer is insignificant lower than in the associated MBL. Elevated layers are showing mean lidar ratios between 41–67 sr, which is in good agreement with typical values of dust and smoke and dust mixtures (Tesche et al., 2011a). At 16° N, 1° S and 12° S, the lidar ratio is slightly higher than the other days while the particle depolarisation is significantly lower, which indicates a mixture with other absorbing, non-depolarising particles like biomass-burning aerosol. The mean particle depolarisation ratio

in the MBL is lower than 1 % in the European influenced Atlantic and the southern hemisphere and show a strong increase in the Saharan influenced region between 35° N and the equator. In this region, depolarising, non-spherical dust particles cause particle depolarisation ratios up to 18 % in the MBL. The mean particle depolarisation in elevated layers is around 30 % at the beginning of the dust plume around 25° N and decreases towards the end, which suggests an increasing mixing with other less depolarising particles. The particle depolarisation ratios of all observed dried marine layers range between 4–9 %. Mean backscatter and extinction-related Ångström exponents range between -0.3 and 2 in the MBL as well as in the elevated layers. A latitudinal difference can be seen in the mean backscatter-related 355/532 nm Ångström exponent of the MBL. The mean $\mathring{A}_{bsc}^{355/532}$ is around 0 in the dust region whereas it is around 1 in the northern and 0.5 in southern latitudes. It can be concluded that there is a mixture of marine aerosol and large dust particles in the MBL between 35° N and the equator whereas in northern and southern mid-latitudes the fraction of smaller particles in the measured marine boundary layers is higher. The mean $\mathring{A}_{bsc}^{355/532}$ in the elevated layers ranges between -0.5 and 0.5 in the region of the dust plumes. A difference between the first and second dust plume is obvious. Between 20 and 30° N, $\mathring{A}_{bsc}^{355/532}$ is negative whereas it became positive during the second plume. According to Veselovskii et al. (2016) a low $\mathring{A}_{bsc}$ indicates an increased imaginary part of the refractive index at 355 nm compared to 532 nm and therefore a higher absorption at 355 nm than at 532 nm. This should be a result from different dust sources and particle properties. The backscatter and extinction-related Ångström exponent of the dried marine layer measured at 31° S are approximately similar to mean values of the MBL. The mean $\mathring{A}_{bsc}^{532/1064}$ in MBL and elevated layers does not show significant latitudinal differences.

The second analysed cruise PS98 provides 18 MBL measurements and eight elevated dust layers. Additionally, one dried marine layer was observed at 23° S. Mean MBL backscatter coefficients at 532 nm range between 1.6–6.5 Mm⁻¹sr⁻¹. In the elevated layers, the mean backscatter coefficient is significantly lower, 0.4–1.7 Mm⁻¹sr⁻¹ at 532 nm. The mean extinction coefficients in the MBL range between 30–180 Mm⁻¹ at 532 nm. Again, the mean extinction coefficient in the dried marine layer is lower than in the MBL and in the same order of magnitude as elevated aerosol layers. Mean values in the MBL are higher in northern latitudes than in southern latitudes, which can be explained with a higher aerosol load in the continental influenced northern hemisphere and the advection of polluted airmasses from Europe. Mean lidar ratios in the MBL range between 13 sr and 34 sr. In contrast to PS95, no significant increase of the MBL lidar ratio in the dust region, between 10° S and 25° N, could be observed. The mixing of dust into the MBL is therefore considered to be low. This is confirmed by a continuous low particle depolarisation ratio of less than 1 % at both wavelengths in the MBL throughout the whole cruise. Elevated aerosol layers could be analysed between 10° S and 25° N and show a wide range of mean lidar and particle depolarisation ratios, caused by different particle types in these layers. At 5° S 2500 km from the African coast, the lidar ratio in the height range of 1.5–2.4 km is at both wavelengths around 35 sr considerable lower than characteristic values of pure dust ($S_{532} \approx 55$ sr (Tesche et al., 2011a)). This may result from marine aerosol transported upward by turbulent mixing processes (Haarig et al., 2017). The upper aerosol layers on 15° N and 19° N show a high lidar ratio (65 sr and 88 sr at 532 nm, respectively). At the same time, the depolarisation ratio is low (11 % and 4 % at 532 nm, respectively) indicating a high fraction of non-depolarising, highly absorbing aerosol like soot. Mean lidar ratios in the other analysed elevated layers range between 40–60 sr at 532 nm. Mean particle depolarisation ratio ranges between 15–26 % at 532 nm. These values are characteristic for dust and biomass-burning aerosol mixtures ($\delta^{par}=$

12–23 % (Groß et al., 2011)) and correspond to a dust fraction of 44 % to 84 %. The dried marine layer during this cruise shows a lidar ratio around 40 sr and particle depolarisation of 5 %. Mean extinction and backscatter-related $Å^{355/532}$ range between -0.5 and 3 and -0.5 and 1.5, respectively. In dusty layers the mean $Å$ is generally smaller than in the MBL, an exception is the upper layer 19° N. In this layer, small soot particles cause a high $Å_{bsc}^{355/532}$. In the dried marine layer, the Ångström exponents

5 are around 1, they are significantly higher than marine values on the same day, indicating smaller particles, but do not show a clear difference to other MBL mean values.

In conclusion one can state, that differences in optical aerosol properties between northern and southern latitudes and the dust-influenced region west of the Saharan dessert could be detected. Whereas the northern hemisphere is influenced by anthropogenic pollution, southern latitudes are more likely to be only marine influenced. Nevertheless, pure marine conditions,

10 not influenced by aerosol originating from the continent, are rare and could only be observed at the end of PS95 near South Africa. Mostly, low-level clouds at top of the MBL at the southern latitudes prohibited the lidar data analysis and thus the evaluation of more cases of pure marine conditions. Cloud cover was about 65 % in the southern hemisphere and 50 % in total during the two cruises.

Dried marine layers at top of the MBL, characterised by a sharp increase of the particle depolarisation, were observed during

15 both cruises. The particle depolarisation ratio in these layers range between 4–9 % and are in good agreement with previous observations (Murayama et al., 1999; Sakai et al., 2000, 2010). A clear difference of the dried marine layers in lidar ratio and Ångström exponent mean values to MBL measurements could not be observed.

4.2 Optical properties for particle typing

20 Mean values of optical properties of the MBL and elevated aerosol layers from PS95 and PS98 (shown in Fig.14) are discussed to illustrate the potential of aerosol classification using intensive optical quantities. Similar classifications for different aerosol types have been shown e.g. by Giannakaki et al. (2010, 2016) and Burton et al. (2012).

In Fig. 15, the lidar ratio at 355 nm (532 nm) is plotted against the particle depolarisation ratio at 355 nm (532 nm). Error bars were omitted for the sake of clarity. The class MBL mixture represent the MBL cases with a significant amount of particles

25 causing enhanced depolarisation. Dusty mixtures are elevated aerosol layers consisting of dust and other non-depolarising particles.

A clear separation of marine and dust influenced MBL measurements can be seen. Pure marine MBL measurements show lidar ratios between 13 sr and 40 sr and particle depolarisation ratios less than 2.5 % at 355 and 532 nm, whereas the particle depolarisation ratio of dust influenced MBL measurements ranges between 5–20 %, caused by a significant amount of non-

30 spherical particles in the MBL. The lidar ratio within these layers also show a tendency to higher lidar ratios with increasing particle depolarisation, caused by the dust particles. Elevated aerosol layer measurements can be divided into layers with a high particle depolarisation ratio (20–30 %) and a lidar ratio of about 50–60 sr, layers with a lidar ratio between 30 sr and 75 sr and a moderate particle depolarisation ratio (<20 %) and layers with a high lidar ratio (>80 sr) and a low particle depolarisation ratio (<10 %). The first category is considered for pure dust cases, whereas the mixing with other non-depolarising particles are

the second category. These particles could be spherical marine particles or biomass-burning aerosol. Is the lidar ratio higher than reference values of pure dust ($\approx$55 sr), the aerosol is considered to be soot, a lower lidar ratio indicate a mixture with marine particles. Layers in the third category with lidar ratios greater than 80 sr and a particle depolarisation lower than 10 % are considered as smoke dominated. As clearly seen, some of the mixed aerosol states do overlap and a clear separation by the

5   lidar ratio and depolarisation ratio is not possible.

Therefore, to complete the picture of particle-type dependent optical properties, in Fig. 16 the backscatter and extinction-related Ångström exponents at 355/532 nm and the backscatter related Ångström exponent at 532/1064 nm are considered for particle type separation in addition to the lidar and depolarisation ratio. The backscatter and extinction-related Ångström exponents as a function of the particle depolarisation ratio (Fig. 16 bottom side) show that the Ångström exponent is not a suitable parameter

10   for the separation of pure marine and dust influenced MBL while a clear separation is possible considering the depolarisation ratio (pure marine: δ^{par}<5 %; aerosol mixtures in the MBL: 5 %< δ^{par}<20 %). For elevated aerosol layers, a slight tendency towards negative backscatter-related Ångström exponents at 355/532 nm with increasing depolarisation ratio values can be seen (Fig. 16 A, C). The extinction-related Ångström exponent at both depolarisation wavelengths is more widely dispersed than the backscatter-related, but show similar patterns (Fig. 16 B, D). In the illustration of the backscatter-related Ångström exponent

15   at 532/1064 nm against the particle depolarisation ratio at 532 nm (Fig. 16 E) no tendency to smaller Ångström exponents with higher depolarisation ratio of the elevated aerosol layers can be observed, thus this parameter is obviously not suitable for a distinction between the different aerosol types. Considering the lidar ratio as a function of the backscatter and extinction-related Ångström exponents (Fig. 16 right side), it again becomes obvious that the Ångström exponent is a much less powerful parameter for aerosol typing in a marine environment compared to the lidar ratio and depolarisation ratio.

20   Resulting from the preceding investigations, we consider the lidar ratio together with the particle depolarisation ratio as best indicators for particle classification above the Atlantic. A clear characteristic in terms of lidar ratio and Ångström exponent for the dried marine layers is not visible. Further observations of those layers are needed to get a comprehensive picture of dried marine aerosol properties.

The values presented above might be valuable information for new aerosol typing schemes needing knowledge from marine

25   areas at the specific lidar wavelengths as for example for the upcoming EarthCARE mission whose lidar will measure at 355 nm.

5   Conclusions

Multiwavelength-Raman-polarisation lidar measurements from two ship-borne cruises across the Atlantic Ocean were analysed. Pure marine, pure dust and dust-smoke mixed conditions were observed. The MBL was often mixed with dust near the

30   equator whereas in the outer tropics the marine influence dominated.

One highlight was the observation of dried marine aerosol at the top of the MBL which were relatively often observed during the cruises aboard RV Polarstern but are rarely reported in literature so far. Dried marine particles cause a particle depolarisation ratios up to 9 % correlated with a decreasing relative humidity under 50 %.

In the northern tropics, west of the Saharan desert, various aerosol layers could be observed during the cruises across the Atlantic from North to South in the frame of the OCEANET project. Besides a pure Saharan dust plume with a negative backscatter-related Ångström exponent of -0.4 ± 0.1 at 355/532 nm near the Canary Islands, Saharan dust layers partly mixed with biomass-burning smoke were observed near the Cape Verde Islands and intensively discussed.

5 A statistical analysis showed latitudinal trends and the potential of aerosol classification of these cruises. Latitudinal differences in the optical properties within the MBL, caused by the down-mixing of dust in the tropics and anthropogenic influences in the northern latitudes, were observed. In the southern hemisphere, the optical properties of the MBL correlate with typical marine values. The mixing of dust in the MBL was low, confirmed by a continuous particle depolarisation ratio of less than 1 % in the MBL in the southern hemisphere. On both cruises, the MBL-top never exceeded 900 m. Elevated aerosol layers were mainly

10 observed in the northern hemisphere tropics and reached up to 4 km. Layers of dried non-spherical marine aerosol on top of the MBL could be observed only a few times, since in about 65 % of the time in southern hemispheric mid-latitudes, low-level clouds prohibited the processing of the lidar data concerning aerosol properties.

All 45 night measurements from PS95 and PS98 were used to illustrate dependencies between lidar ratio, particle depolar-

15 isation ratio and Ångström exponent for the different aerosol types. Lidar ratio and particle depolarisation ratio have been found to be the main indicator for the characterisation of the particle types observed over the Atlantic, whereas the Ångström exponent is rather variable. Marine, dust and smoke aerosols could be clearly identified with this parameter. Care must be taken when layers of dried marine aerosol occur at the top of the MBL, as the enhanced depolarisation ratio (4-9 %) could lead to wrong conclusions concerning the mixing state of the aerosol (wrong to attribution to mineral dust occurrence). We therefore

20 recommend to consider the relative humidity and the vertical connection to marine layers when performing aerosol typing above the Ocean.

The values obtained increase the knowledge of the aerosol conditions in marine environments which make 70 % of the Earth's surface. Therefore the presented results may also be a valuable contribution for the data analysis of satellite retrievals which are the only instruments able to cover this large part of the Earth at the moment. The obtained data can also be used to validate

25 and further improve model calculations e.g. by evaluation of the height of the different aerosol layers.

Data availability. Meteorological data of all RV Polarstern cruises are available on the Pangaea data base (https://www.pangaea.de). For lidar data analysis, GDAS1 (Global Data Assimilation System) height profiles of the National Weather Service's National Centers for Environmental Prediction (NCEP) were used (https://www.ncdc.noaa.gov/data-access/model-data/model-datasets/global-data-assimilation-system-gdas). Trajectories are calculated with the NOAA (National Oceanic and Atmospheric Administration) HYSPLIT (HYbrid Single-Particle La-

30 grangian Integrated Trajectory) model (https://ready.arl.noaa.gov/HYSPLIT.php). The additionally shown fire data detected by MODIS (Moderate Resolution Imaging Spectroradiometer) are available at: https://lance.modaps.eosdis.nasa.gov/firemaps. AOT data can be downloaded from the AERONET Maritime Aerosol Network (MAN) data base (https://aeronet.gsfc.nasa.gov/new_web/maritime_aerosol_network.html). The RV Polarstern lidar data are available upon request at TROPOS (http://polly.tropos.de).

Acknowledgements. The authors acknowledge support through ACTRIS under grant agreement No 262254 and ACTRIS-2 under grant agreement No 654109 from the European Union's Horizon 2020 research and innovation programme. We thank the team of RV Polarstern and the German Weather Service (DWD) for their support during the cruises PS95 and PS98. We appreciate the effort of AERONET MAN to enable sun photometer measurements on research vessels.

References

Albrecht, B. A.: Aerosols, cloud microphysics, and fractional cloudiness, Science, 245, 1227–1230, doi:10.1126/science.245.4923.1227, http://www.sciencemag.org/cgi/content/abstract/245/4923/1227, 1989.

Althausen, D., Engelmann, R., Baars, H., Heese, B., Ansmann, A., Müller, D., and Komppula, M.: Portable Raman lidar Polly[XT] for automated profiling of aerosol backscatter, extinction, and depolarization, Journal of Atmospheric and Oceanic Technology, 26, 2366–2378, doi:10.1175/2009JTECHA1304.1, http://ams.allenpress.com/perlserv/?request=get-abstract&doi=10.1175%2F2009JTECHA1304.1, 2009.

Ångström, A.: On the Atmospheric Transmission of Sun Radiation and on Dust in the Air, Geografiska Annaler, 11, pp. 156–166, 1929.

Baars, H., Kanitz, T., Engelmann, R., Althausen, D., Heese, B., Komppula, M., Preißler, J., Tesche, M., Ansmann, A., Wandinger, U., Lim, J.-H., Ahn, J. Y., Stachlewska, I. S., Amiridis, V., Marinou, E., Seifert, P., Hofer, J., Skupin, A., Schneider, F., Bohlmann, S., Foth, A., Bley, S., Pfüller, A., Giannakaki, E., Lihavainen, H., Viisanen, Y., Hooda, R. K., Pereira, S. N., Bortoli, D., Wagner, F., Mattis, I., Janicka, L., Markowicz, K. M., Achtert, P., Artaxo, P., Pauliquevis, T., Souza, R. A. F., Sharma, V. P., van Zyl, P. G., Beukes, J. P., Sun, J., Rohwer, E. G., Deng, R., Mamouri, R.-E., and Zamorano, F.: An overview of the first decade of Polly[NET]: an emerging network of automated Raman-polarization lidars for continuous aerosol profiling, Atmospheric Chemistry and Physics, 16, 5111–5137, doi:10.5194/acp-16-5111-2016, http://www.atmos-chem-phys.net/16/5111/2016/, 2016.

Bösenberg, J., Hoff, R., Ansmann, A., Müller, D., Antuña, J. C., Whiteman, D., Sugimoto, N., Apituley, A., Hardesty, M., Welton, J., Eloranta, E., Arshinov, Y., Kinne, S., and Freudenthaler, V.: Plan for the implementation of the GAW Aerosol Lidar Observation Network GALION, GAW No. 178, 2007.

Burton, S. P., Ferrare, R. A., Hostetler, C. A., Hair, J. W., Rogers, R. R., Obland, M. D., Butler, C. F., Cook, A. L., Harper, D. B., and Froyd, K. D.: Aerosol classification using airborne High Spectral Resolution Lidar measurements – methodology and examples, Atmospheric Measurement Techniques, 5, 73–98, doi:10.5194/amt-5-73-2012, https://www.atmos-meas-tech.net/5/73/2012/, 2012.

Eck, T. F., Holben, B. N., Reid, J. S., Dubovik, O., Smirnov, A., O'Neill, N. T., Slutsker, I., and Kinne, S.: Wavelength dependence of the optical depth of biomass burning, urban, and desert dust aerosols, Journal of Geophysical Research: Atmospheres, 104, 31 333–31 349, doi:10.1029/1999JD900923, http://dx.doi.org/10.1029/1999JD900923, 1999.

Engelmann, R., Kanitz, T., Baars, H., Heese, B., Althausen, D., Skupin, A., Wandinger, U., Komppula, M., Stachlewska, I. S., Amiridis, V., Marinou, E., Mattis, I., Linné, H., and Ansmann, A.: The automated multiwavelength Raman polarization and water-vapor lidar Polly[XT]: the neXT generation, Atmospheric Measurement Techniques, 9, 1767–1784, doi:10.5194/amt-9-1767-2016, http://www.atmos-meas-tech.net/9/1767/2016/, 2016.

Giannakaki, E., Balis, D. S., Amiridis, V., and Zerefos, C.: Optical properties of different aerosol types: seven years of combined Raman-elastic backscatter lidar measurements in Thessaloniki, Greece, Atmospheric Measurement Techniques, 3, 569–578, doi:10.5194/amt-3-569-2010, https://www.atmos-meas-tech.net/3/569/2010/, 2010.

Giannakaki, E., van Zyl, P. G., Müller, D., Balis, D., and Komppula, M.: Optical and microphysical characterization of aerosol layers over South Africa by means of multi-wavelength depolarization and Raman lidar measurements, Atmospheric Chemistry and Physics, 16, 8109–8123, doi:10.5194/acp-16-8109-2016, https://www.atmos-chem-phys.net/16/8109/2016/, 2016.

Groß, S., Tesche, M., Freudenthaler, V., Toledano, C., Wiegner, M., Ansmann, A., Althausen, D., and Seefeldner, M.: Characterization of Saharan dust, marine aerosols and mixtures of biomass–burning aerosols and dust by means of multi–wavelength depolarization and

Raman lidar measurements during SAMUM 2, Tellus B, 63, doi:10.1111/j.1600-0889.2011.00556.x, http://www.tellusb.net/index.php/tellusb/article/view/16369, 2011.

Haarig, M., Ansmann, A., Gasteiger, J., Kandler, K., Althausen, D., Baars, H., Radenz, M., and Farrell, D. A.: Dry versus wet marine particle optical properties: RH dependence of depolarization ratio, backscatter, and extinction from multiwavelength lidar measurements during SALTRACE, Atmospheric Chemistry and Physics, 17, 14 199–14 217, doi:10.5194/acp-17-14199-2017, https://www.atmos-chem-phys.net/17/14199/2017/, 2017.

IPCC: Climate Change 2013: The Physical Science Basis. Contribution of Working Group I to the Fifth Assessment Report of the Intergovernmental Panel on Climate Change, Cambridge University Press, 589 pp., 2013.

Kanitz, T.: Vertical distribution of aerosols above the Atlantic Ocean, Punta Arenas (Chile), and Stellenbosch (South Africa). Characterization, solar radiative effects and ice nucleating properties, Ph.D. thesis, Technische Universität Berlin, http://www.tropos.de/fileadmin/user_upload/Institut/Abteilungen/Fernerkundung/Daten_PDF/dissertation_kanitz.pdf, available at: http://www.tropos.de/en/institute/departments/remote-sensing-of-atmospheric-processes-new/ground-based-remote-sensing/academical-degrees/, 2012.

Kokhanovsky, A.: Aerosol Optics: Light Absorption and Scattering by Particles in the Atmosphere, Springer Praxis Books, Springer Berlin Heidelberg, https://books.google.de/books?id=QEmRH5T11yUC, 2008.

Müller, D., Ansmann, A., Mattis, I., Tesche, M., Wandinger, U., Althausen, D., and Pisani, G.: Aerosol–type–dependent lidar ratios observed with Raman lidar, Journal of Geophysical Research: Atmospheres, 112, D16 202, doi:10.1029/2006JD008292, http://www.agu.org/pubs/crossref/2007/2006JD008292.shtml, 2007.

Murayama, T., Okamoto, H., Kaneyasu, N., Kamataki, H., and Miura, K.: Application of lidar depolarization measurement in the atmospheric boundary layer: Effects of dust and sea-salt particles, Journal of Geophysical Research: Atmospheres, 104, 31 781–31 792, doi:10.1029/1999JD900503, http://dx.doi.org/10.1029/1999JD900503, 1999.

Myhre, G., Samset, B. H., Schulz, M., Balkanski, Y., Bauer, S., Berntsen, T. K., Bian, H., Bellouin, N., Chin, M., Diehl, T., Easter, R. C., Feichter, J., Ghan, S. J., Hauglustaine, D., Iversen, T., Kinne, S., Kirkevåg, A., Lamarque, J.-F., Lin, G., Liu, X., Lund, M. T., Luo, G., Ma, X., van Noije, T., Penner, J. E., Rasch, P. J., Ruiz, A., Seland, Ø., Skeie, R. B., Stier, P., Takemura, T., Tsigaridis, K., Wang, P., Wang, Z., Xu, L., Yu, H., Yu, F., Yoon, J.-H., Zhang, K., Zhang, H., and Zhou, C.: Radiative forcing of the direct aerosol effect from AeroCom Phase II simulations, Atmospheric Chemistry and Physics, 13, 1853–1877, doi:10.5194/acp-13-1853-2013, http://www.atmos-chem-phys.net/13/1853/2013/, 2013.

Nisantzi, A., Mamouri, R. E., Ansmann, A., and Hadjimitsis, D.: Injection of mineral dust into the free troposphere during fire events observed with polarization lidar at Limassol, Cyprus, Atmospheric Chemistry and Physics, 14, 12 155–12 165, doi:10.5194/acp-14-12155-2014, http://www.atmos-chem-phys.net/14/12155/2014/, 2014.

Ocko, I. B., Ramaswamy, V., Ginoux, P., Ming, Y., and Horowitz, L. W.: Sensitivity of scattering and absorbing aerosol direct radiative forcing to physical climate factors, Journal of Geophysical Research: Atmospheres, 117, doi:10.1029/2012JD018019, http://dx.doi.org/10.1029/2012JD018019, d20203, 2012.

Omar, A. H., Winker, D. M., Kittaka, C., Vaughan, M. A., Liu, Z., Hu, Y., Trepte, C. R., Rogers, R. R., Ferrare, R. A., Lee, K.-P., Kuehn, R. E., and Hostetler, C. A.: The CALIPSO automated aerosol classification and lidar ratio selection algorithm, Journal of Atmospheric and Oceanic Technology, 26, 1994, doi:10.1175/2009JTECHA1231.1, http://ams.allenpress.com/perlserv/?request=get-abstract&doi=10.1175%2F2009JTECHA1231.1, 2009.

Rittmeister, F., Ansmann, A., Engelmann, R., Skupin, A., Baars, H., Kanitz, T., and Kinne, S.: Profiling of Saharan dust from the Caribbean to western Africa – Part 1: Layering structures and optical properties from shipborne polarization/Raman lidar observations, Atmospheric Chemistry and Physics, 17, 12 963–12 983, doi:10.5194/acp-17-12963-2017, https://www.atmos-chem-phys.net/17/12963/2017/, 2017.

Sakai, T., Shibata, T., Kwon, S.-A., Kim, Y.-S., Tamura, K., and Iwasaka, Y.: Free tropospheric aerosol backscatter, depolarization ratio, and relative humidity measured with the Raman lidar at Nagoya in 1994–1997: contributions of aerosols from the Asian Continent and the Pacific Ocean, Atmospheric Environment, 34, 431–442, doi:10.1016/S1352-2310(99)00328-3, http://www.sciencedirect.com/science/article/pii/S1352231099003283, 2000.

Sakai, T., Nagai, T., Zaizen, Y., and Mano, Y.: Backscattering linear depolarization ratio measurements of mineral, sea-salt, and ammonium sulfate particles simulated in a laboratory chamber, Appl. Opt., 49, 4441–4449, doi:10.1364/AO.49.004441, http://ao.osa.org/abstract.cfm?URI=ao-49-23-4441, 2010.

Smirnov, A., Holben, B. N., Slutsker, I., Giles, D. M., McClain, C. R., Eck, T. F., Sakerin, S. M., Macke, A., Croot, P., Zibordi, G., Quinn, P. K., Sciare, J., Kinne, S., Harvey, M., Smyth, T. J., Piketh, S., Zielinski, T., Proshutinsky, A., Goes, J. I., Nelson, N. B., Larouche, P., Radionov, V. F., Goloub, P., Krishna Moorthy, K., Matarrese, R., Robertson, E. J., and Jourdin, F.: Maritime Aerosol Network as a component of Aerosol Robotic Network, Journal of Geophysical Research: Atmospheres, 114, doi:10.1029/2008JD011257, http://dx.doi.org/10.1029/2008JD011257, d06204, 2009.

Tesche, M., Ansmann, A., Müller, D., Althausen, D., Engelmann, R., Freudenthaler, V., and Groß, S.: Vertically resolved separation of dust and smoke over Cape Verde using multiwavelength Raman and polarization lidars during Saharan Mineral Dust Experiment 2008, Journal of Geophysical Research, 114, D13 202, doi:10.1029/2009JD011862, 2009.

Tesche, M., Groß, S., Ansmann, A., Müller, D., Althausen, D., Freudenthaler, V., and Esselborn, M.: Profiling of Saharan dust and biomass-burning smoke with multiwavelength polarization Raman lidar at Cape Verde, Tellus B, 63, http://www.tellusb.net/index.php/tellusb/article/view/16360, 2011a.

Tesche, M., Müller, D., Groß, S., Ansmann, A., Althausen, D., Freudenthaler, V., Weinzierl, B., Veira, A., and Petzold, A.: Optical and microphysical properties of smoke over Cape Verde inferred from multiwavelength lidar measurements, Tellus B, 63, 677–694, doi:10.1111/j.1600-0889.2011.00549.x, http://dx.doi.org/10.1111/j.1600-0889.2011.00549.x, 2011b.

Tsekeri, A., Lopatin, A., Amiridis, V., Marinou, E., Igloffstein, J., Siomos, N., Solomos, S., Kokkalis, P., Engelmann, R., Baars, H., Gratsea, M., Raptis, P. I., Binietoglou, I., Mihalopoulos, N., Kalivitis, N., Kouvarakis, G., Bartsotas, N., Kallos, G., Basart, S., Schuettemeyer, D., Wandinger, U., Ansmann, A., Chaikovsky, A. P., and Dubovik, O.: GARRLiC and LIRIC: strengths and limitations for the characterization of dust and marine particles along with their mixtures, Atmospheric Measurement Techniques, 10, 4995–5016, doi:10.5194/amt-10-4995-2017, https://www.atmos-meas-tech.net/10/4995/2017/, 2017.

Twomey, S.: The Influence of Pollution on the Shortwave Albedo of Clouds, Journal of Atmospheric Science, 34, 1149–1154, 1977.

Veselovskii, I., Goloub, P., Podvin, T., Bovchaliuk, V., Derimian, Y., Augustin, P., Fourmentin, M., Tanre, D., Korenskiy, M., Whiteman, D. N., Diallo, A., Ndiaye, T., Kolgotin, A., and Dubovik, O.: Retrieval of optical and physical properties of African dust from multi-wavelength Raman lidar measurements during the SHADOW campaign in Senegal, Atmospheric Chemistry and Physics, 16, 7013–7028, doi:10.5194/acp-16-7013-2016, http://www.atmos-chem-phys.net/16/7013/2016/, 2016.

Wandinger, U.: Introduction to Lidar, in: Lidar: Range–Resolved Optical Remote Sensing of the Atmosphere, edited by Weitkamp, C., pp. 1–18, Springer, 2005.
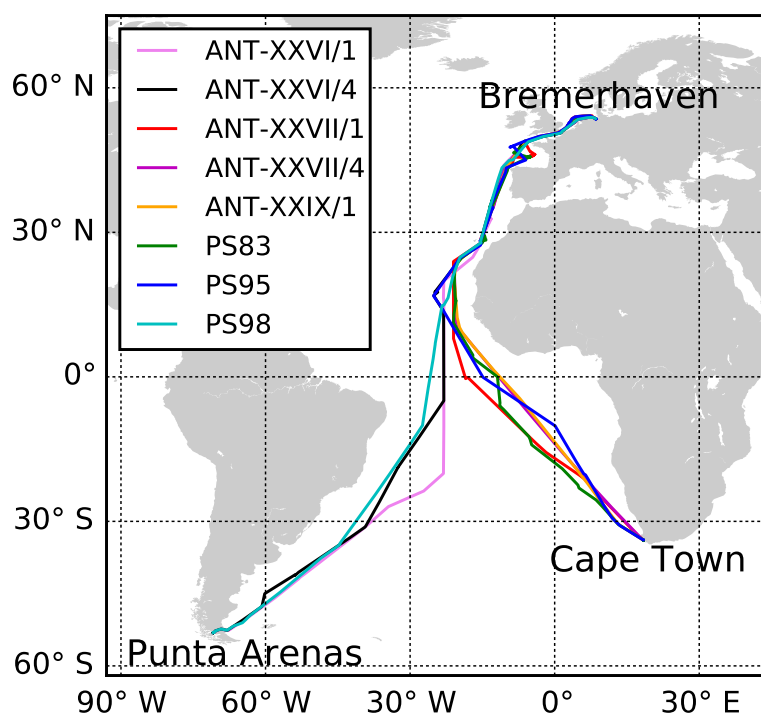
Figure 1. Polarstern cruises with Polly^{XT} aboard until PS98. Cruise tracks are taken from the Pangaea database (https://www.pangaea.de/expeditions/cr.php/Polarstern, accessed: 24/02/2017).
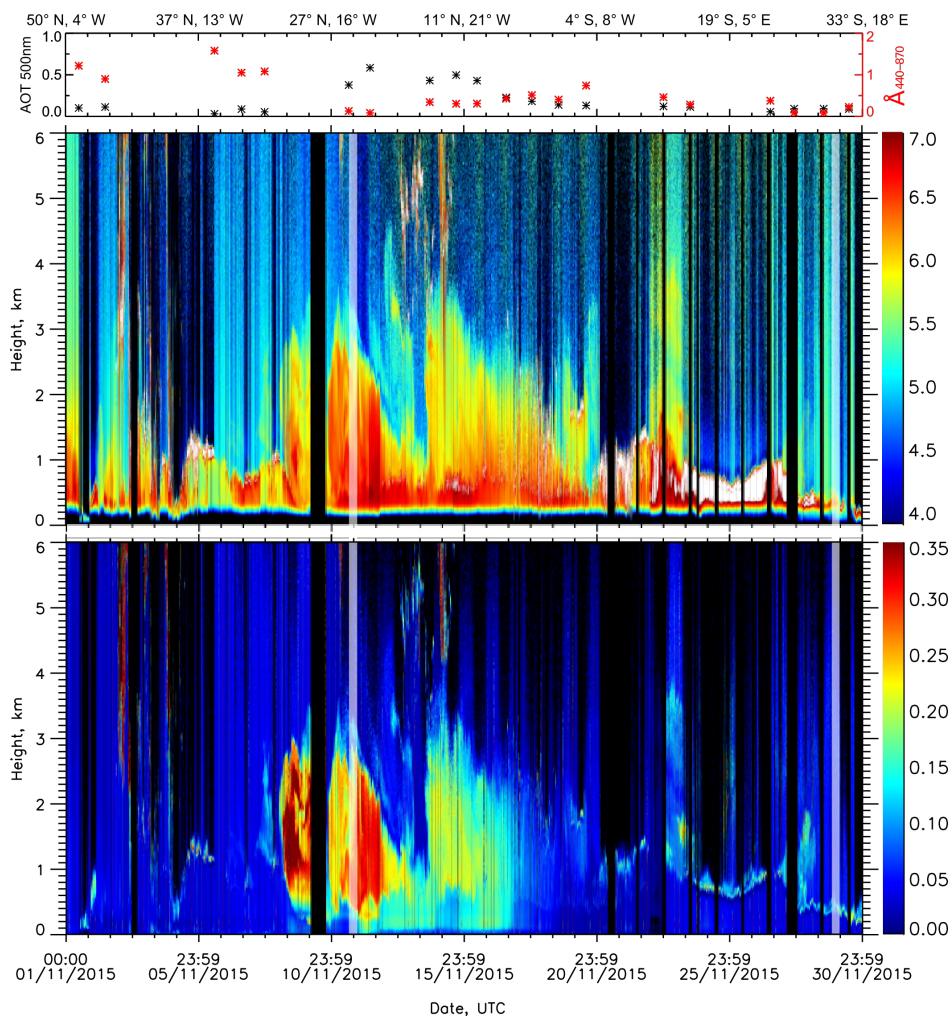
Figure 2. Observational overview of the autumn cruise PS95 from Bremerhaven to Cape Town. Time series of the 500 nm AOT and 440-870 nm Ångström exponent derived with Microtops sunphotometer measurements (upper panel) and height-time display of the 1064 nm range-corrected lidar signal (middle panel) and the volume depolarisation ratio at 532 nm (lower panel).
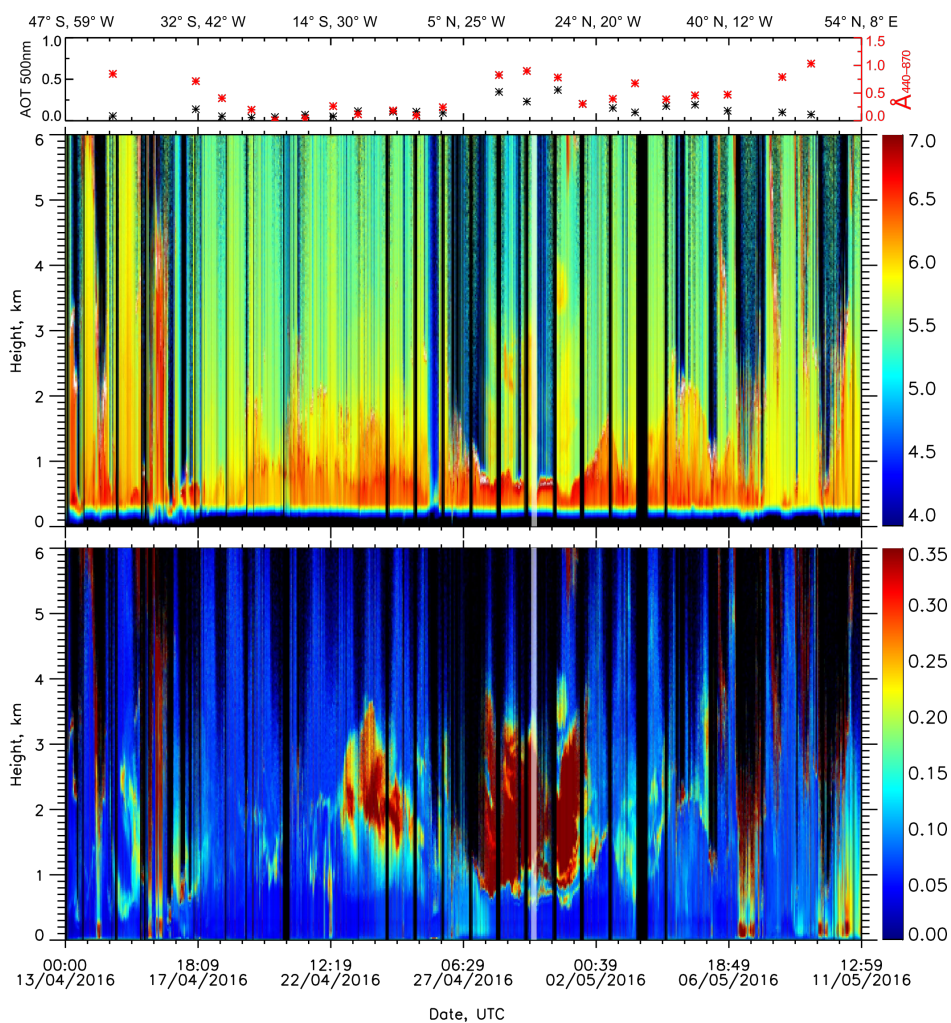
Figure 3. Same as Fig. 2 but for the spring cruise PS98 from Punta Arenas to Bremerhaven. Due to the failure of the 1064 nm channel, the 532 nm range-corrected signal is shown in the middle panel.
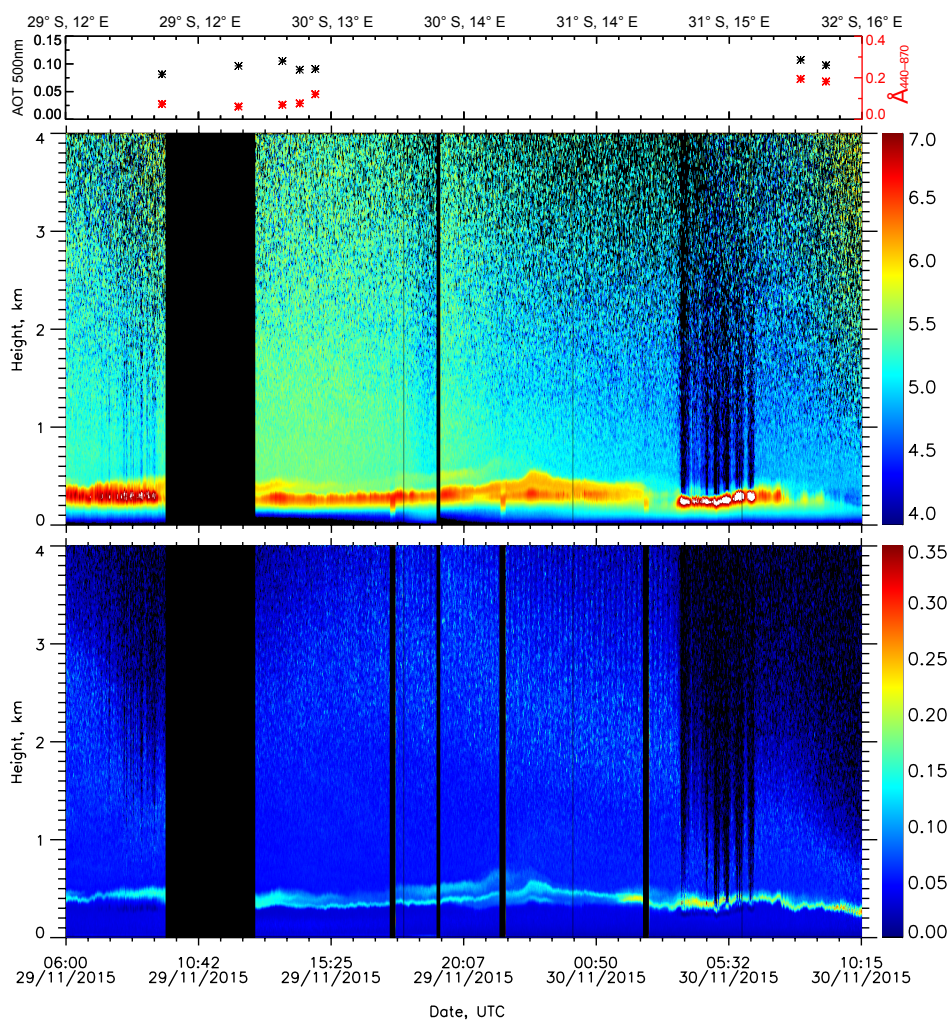
Figure 4. Marine conditions during PS95: time series of the Microtops sun photometer derived AOT at 500 nm and 440/870 nm Ångström exponent (upper panel), 1064 nm range-corrected signal (middle panel) and 532 nm volume depolarisation ratio (lower panel).
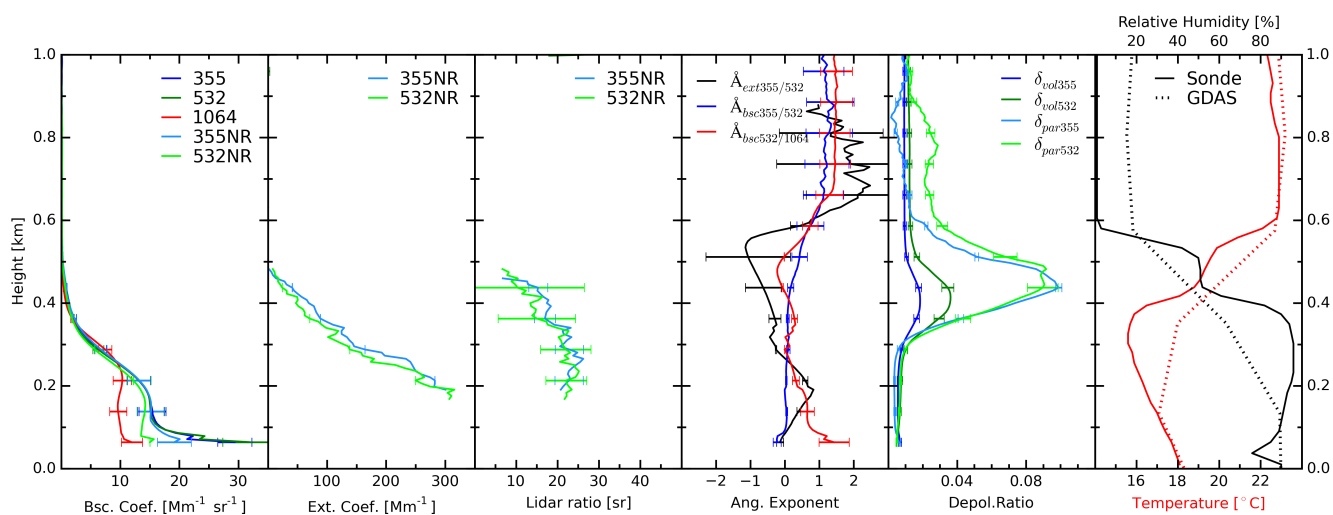
Figure 5. Profiles averaged for 30 November 2015, 01:15–02:30 UTC. Backscatter coefficient and depolarisation ratios smoothed with 127.5 m vertical length. Extinction coefficients, lidar ratios and Ångström exponents are smoothed with 127.5 m up to 242 m and afterwards with 367.5 m. Meteorological data from GDAS1 (30 November 2015, 00 UTC) and radio sounding measurements (29 November 2015, 12 UTC) are also presented.
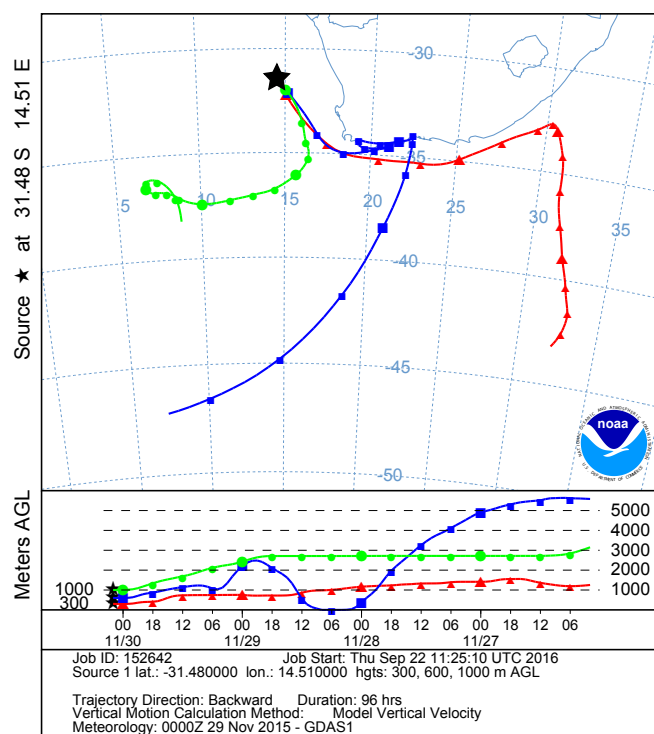
Figure 6. NOAA HYSPLIT backward trajectories for 4 days ending at the position of Polarstern (31.48° S, 14.51° E, marked by the black star) on 30 November 2015, 02:00 UTC at 300 m, 600 m and 1000 m AGL.
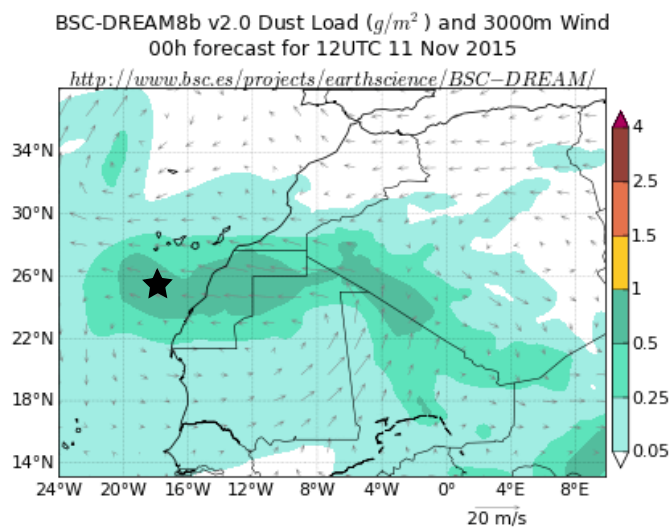
Figure 7. Column integrated dust concentration on 11 November 2015 12:00 UTC from the BSC-DREAM8b model (Dust REgional Atmospheric Model), operated by the Barcelona Supercomputing Center (http://www.bsc.es/ESS/services/ BSC-DREAM8b, accessed: 14/11/1016). The position of Polarstern is marked by the black star.
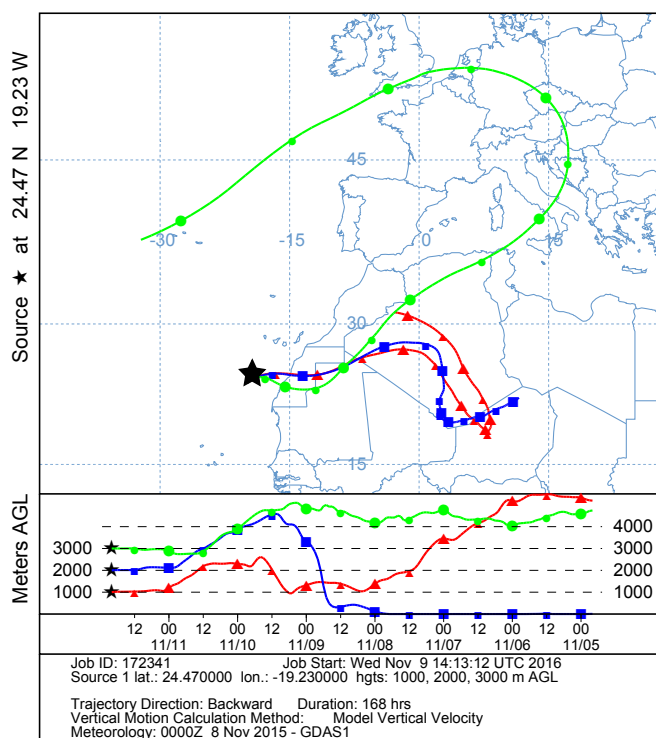
Figure 8. 7-day NOAA HYSPLIT backward trajectories ending at the position of Polarstern on 11 November 2015, 20:00 UTC (24.27° N, 19.23° W). The position of Polarstern is marked by the black star.
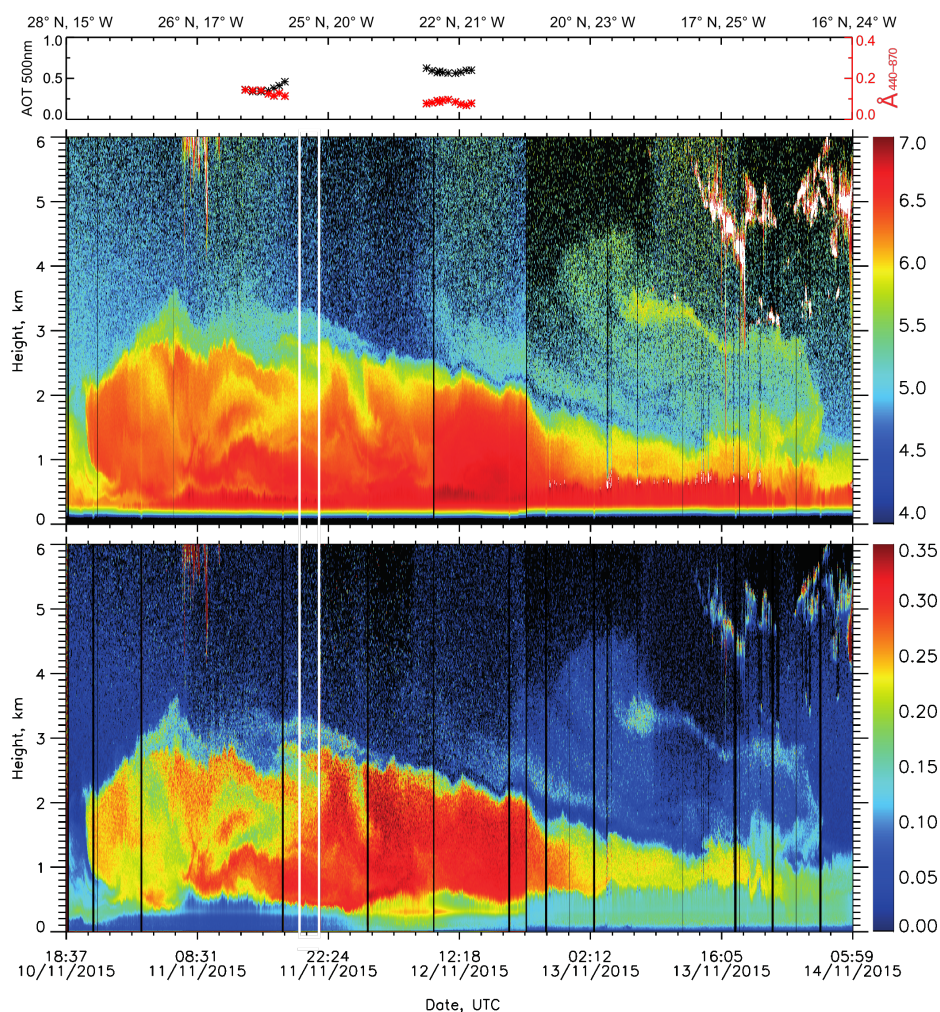
Figure 9. First dust event observed during PS95: time series of the Microtops sun photometer derived AOT (500 nm) and 440/870 nm Ångström exponent (upper panel), 1064 nm range-corrected signal (middle panel) and 532 nm volume depolarisation ratio (lower panel).
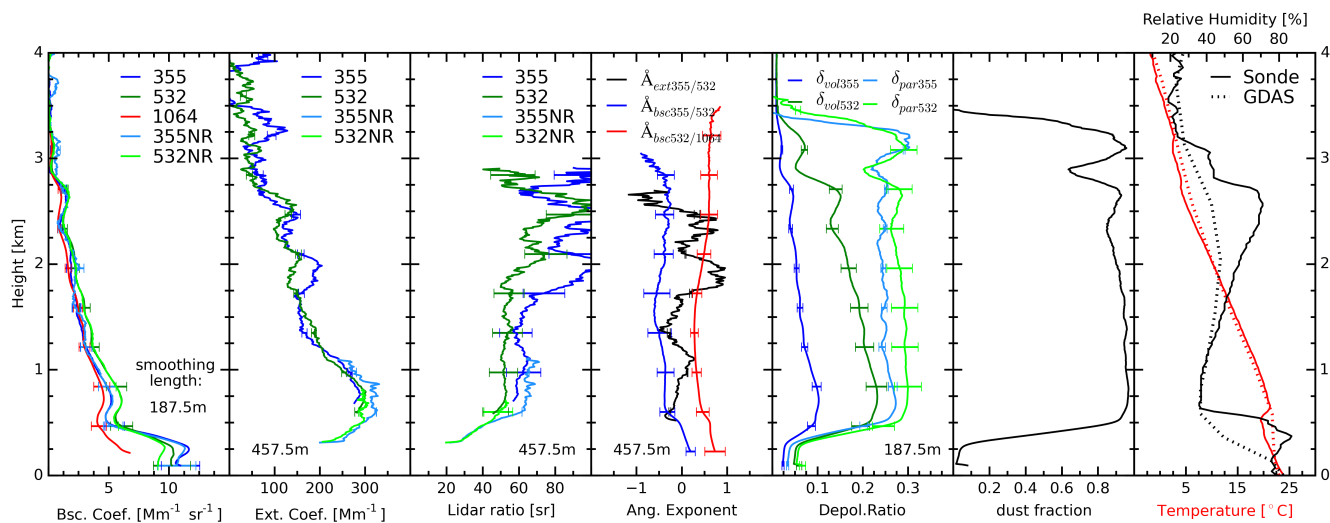
Figure 10. Profiles averaged for 11 November 2015, 19:30–21:00 UTC. Dust fraction calculated after Tesche et al. (2009). Radio sounding profiles from 11 November 2015, 12 UTC and GDAS1 profiles (11 November 2015, 18 UTC) are presented in the right panel.
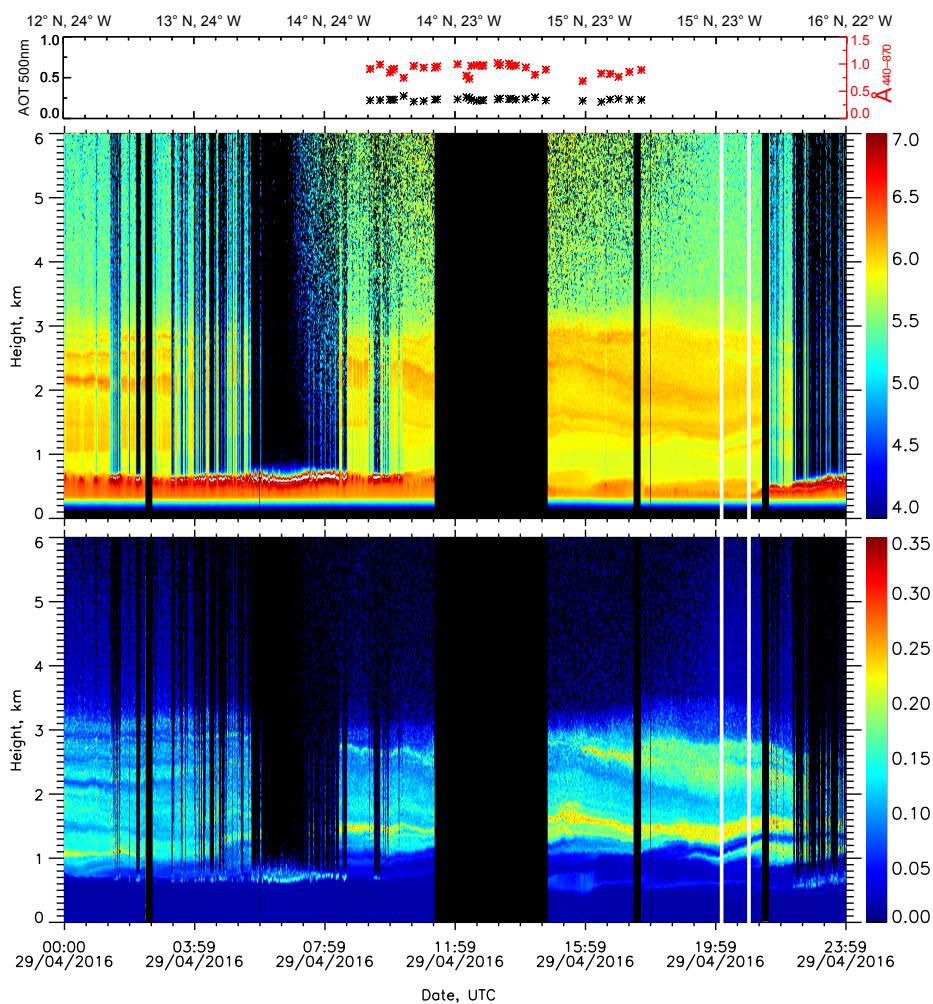
Figure 11. Complex aerosol layering with smoke and dust on PS98: Sun photometer derived AOT at 500 nm and 440/870 nm Ångström exponent (upper panel), 532 nm range-corrected signal (middle panel) and volume depolarisation ratio (lower panel).
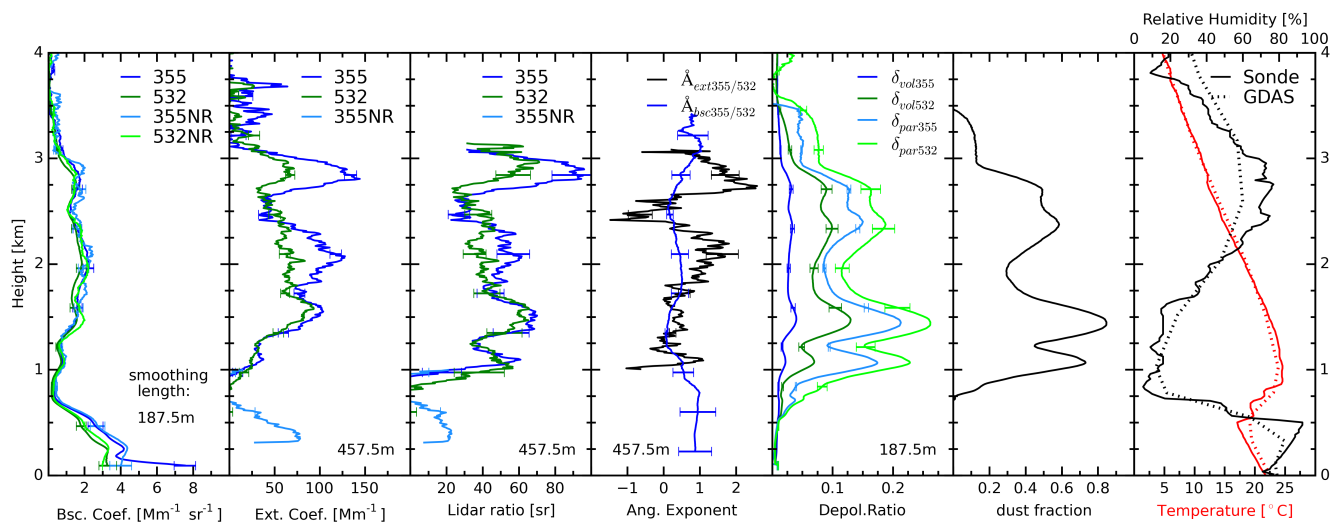
Figure 12. Averaged profiles for 29 April 2016, 20:15–21:00 UTC. Dust fraction calculated after Tesche et al. (2009). Meteorological data from GDAS1 (29 April 2016, 21 UTC) and radio sounding measurements (29 April 2016, 15 UTC).
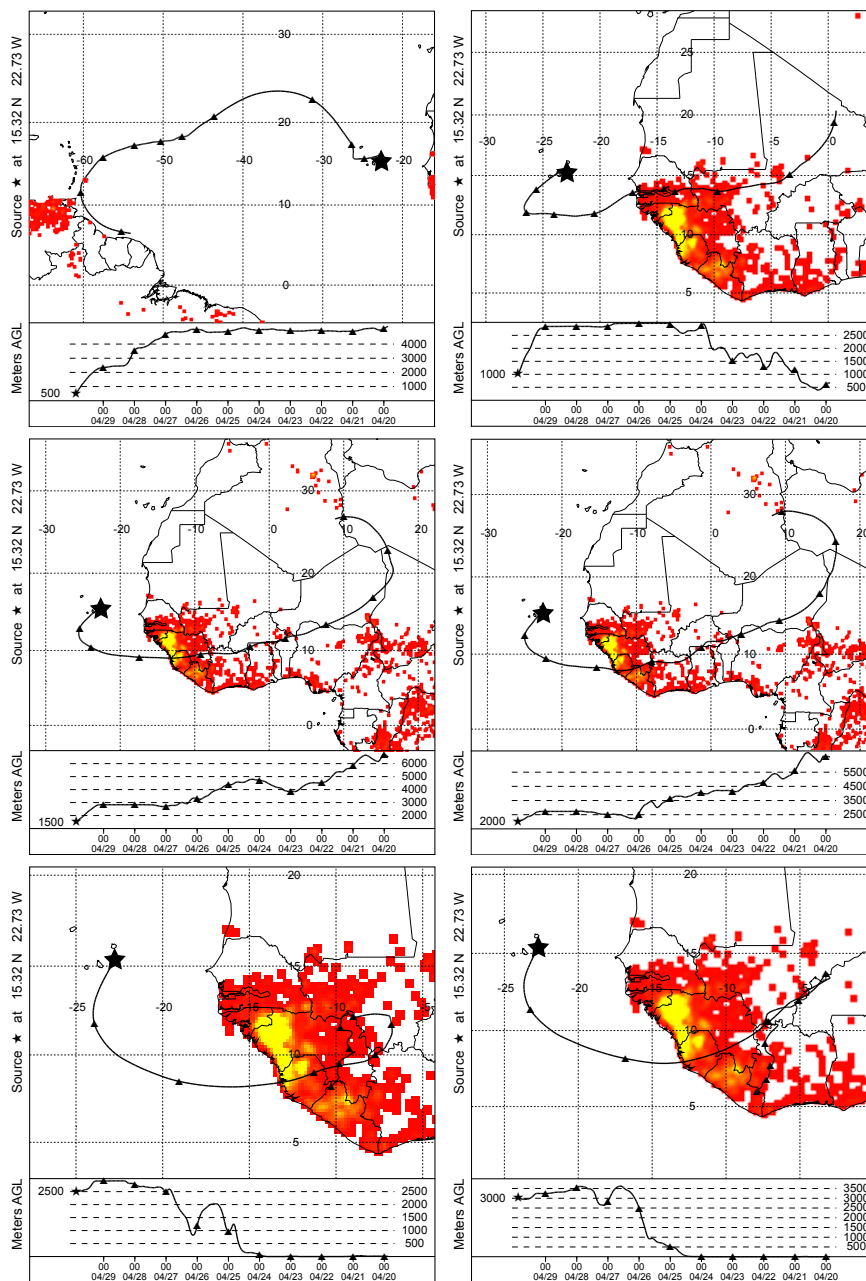
Figure 13. NOAA HYSPLIT backward trajectories ending at 29 April 2016 21:00 UTC at the position of Polarstern (15.32° N, 22.73° W, marked by the black star) at different altitudes. Additionally, fires detected by MODIS on board the Terra and Aqua satellites are shown. Fires are accumulated over the 10-day period from 20 April 2016 to 29 April 2016. Yellow color indicates a large number of fires, red dots indicate a low number of fires in the considered period (https://lance.modaps.eosdis.nasa.gov/firemaps, accessed: 24/02/2017).
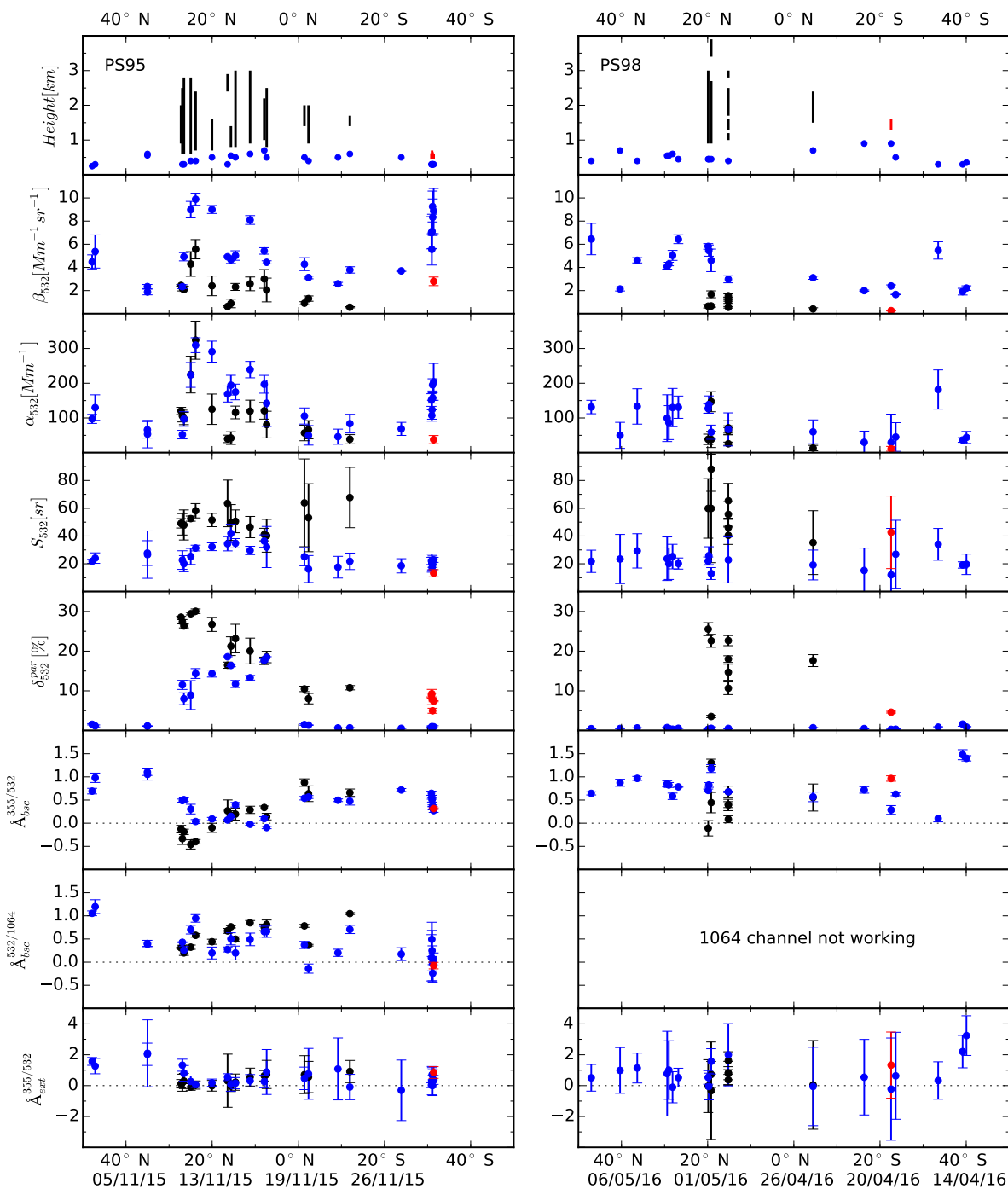
Figure 14. Mean values of the 532 nm backscatter and extinction coefficient, lidar ratio, particle depolarisation ratio and the backscatter-related Ångström exponent at 355/532 nm and 532/1064 nm and the extinction-related Ångström exponent at 355/532 nm (top down) for MBL (blue), elevated aerosol layers (black) and dried marine layers (red) on PS95 (left column) and PS98 (right column) from North to South. Error bars indicate the standard deviation. MBL top height and extent of the elevated layers are shown in the first row.
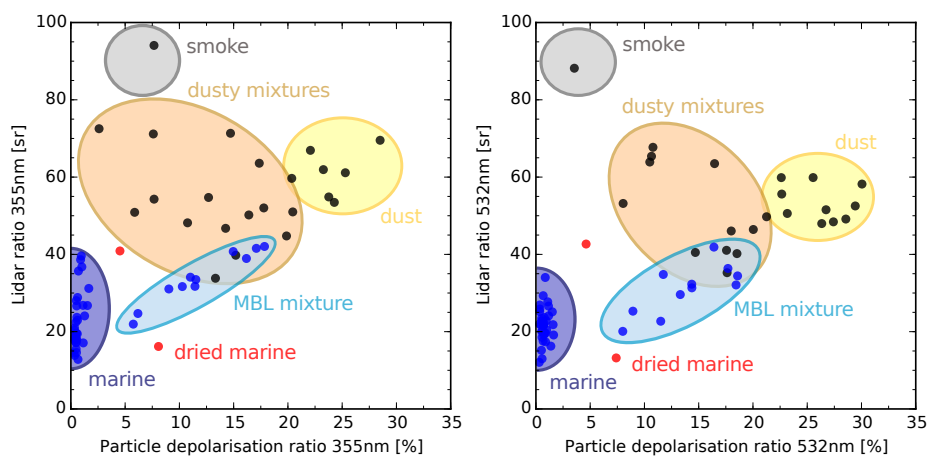
Figure 15. Lidar ratio as a function of the particle depolarisation ratio at 355 nm (left) and at 532 nm (right) from all analysed MBL (blue), elevated aerosol layer (black) and dried marine layer (red) measurements of PS95 and PS98. The classification of the detected aerosols is delineated.
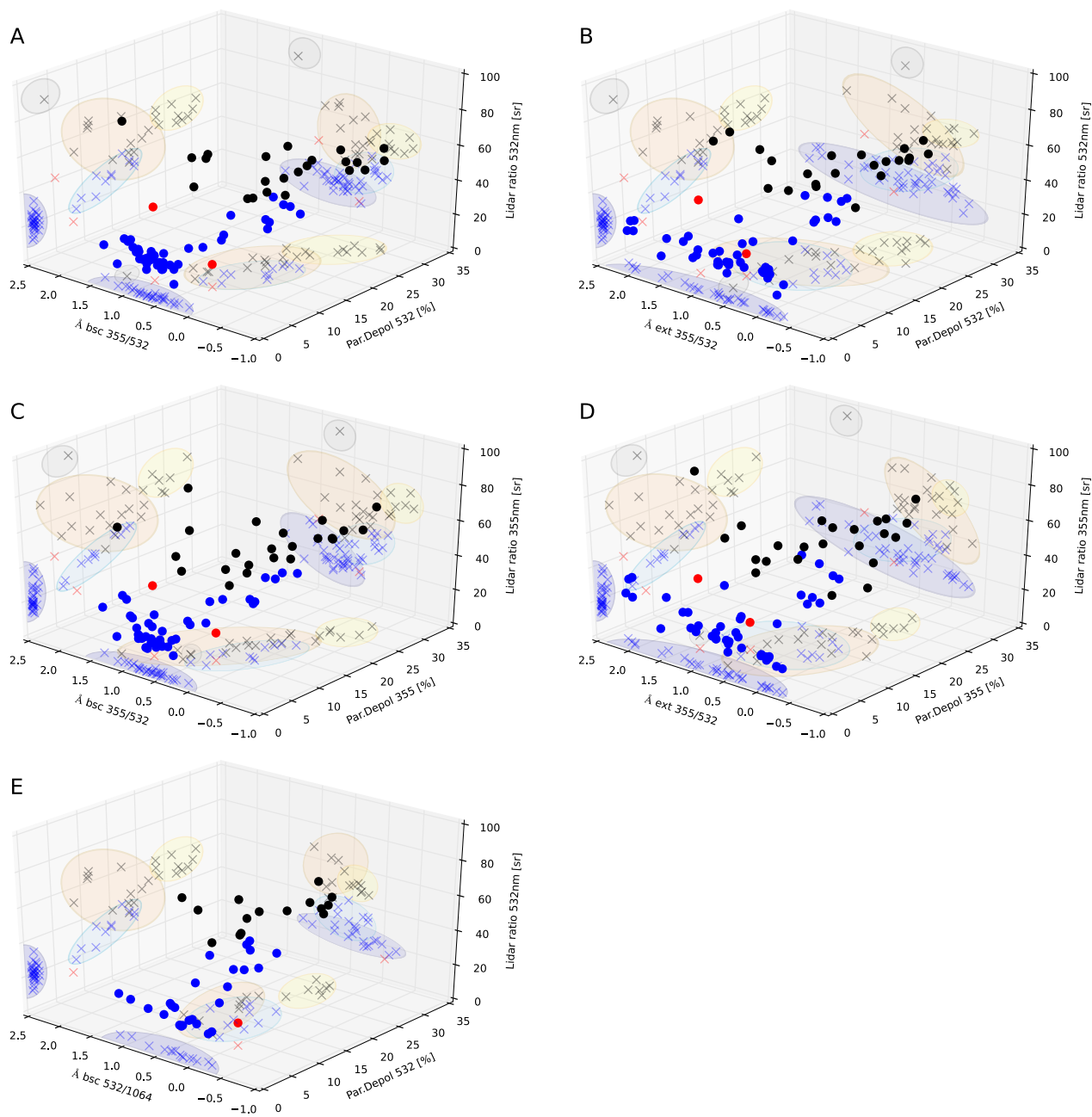
Figure 16. Three-dimensional illustration of the relation between lidar ratio and depolarisation ratio at 355 nm and 532 nm and backscatter and extinction-related Ångström exponent at 355/532 nm and backscatter-related Ångström exponent at 532/1064 nm. Blue dots represent MBL measurements, black dots elevated aerosol layers and red dots dried marine layers.

Table 1: All previous Polarstern cruises with Polly^{XT} aboard between Bremerhaven (BHV) and Cape Town and Bremerhaven and Punta Arenas. From PS83 a new numbering was used.

Cruise label	Time period	Route	Lidar system
ANT-XXVI/1	16 Oct - 25 Nov 2009	BHV - Punta Arenas	Polly^{XT}-IfT
ANT-XXVI/4	7 Apr - 17 May 2010	Punta Arenas - BHV	Polly^{XT}-IfT
ANT-XXVII/1	27 Oct - 25 Nov 2011	BHV - Cape Town	Polly^{XT}-IfT
ANT-XXVII/4	20 Apr - 20 May 2011	Cape Town - BHV	Polly^{XT}-IfT
ANT-XXIX/1	26 Oct - 26 Nov 2012	BHV - Cape Town	Polly^{XT}-OCEANET
PS83	8 Mar - 12 Apr 2014	Cape Town - BHV	Polly^{XT}-OCEANET
PS95	29 Oct - 1 Dec 2015	BHV - Cape Town	Polly^{XT}-OCEANET
PS98	10 Apr - 12 May 2016	Punta Arenas - BHV	Polly^{XT}-OCEANET